INTERNATIONAL CENTER FOR NUMERICAL METHODS IN ENGINEERING

A Finite Element Method for the Solution of Potencial Flow in Two Dimensions

T.M. Hughes
E. Oñate
J. Miquel

Publication, CIMNE Nº 11, July 1991

A Finite Element Method for the Solution of Potencial Flow in Two Dimensions

T.M. Hughes
E. Oñate
J. Miquel

Publication CIMNE Nº-11, July 1991

International Center for Numerical Methods in Engineering
Gran Capitán s/n, 08034 Barcelona, Spain

SUMMARY.

This report presents a method for the solution of two dimensional, potential flow around an aerofoil based on a Finite Element Method for the solution of Laplace's equation. Solutions to approximate the "real" flow are constructed from the observation that potential flow solutions are linear and thus, many potential flows may be superimposed to yield the desired flow. Indeed, in this way, one of the effects of viscosity, that of fixing the rear stagnation point to the trailing edge for up to moderate angle of attack cases, is modelled by the imposition of a potential flow due to a point vortex (located at the 1/4 chord point) sufficient to fix the rear stagnation point at the trailing edge (Kutta condition).

It must be remembered however, that potential flow solutions are inviscid and as such do not model correctly the flow separation point and further, the absence of viscosity falsely causes the model to predict zero drag caused by the aerofoil. However, the predictions made for the lift (derived from the calculated circulation to fix the Kutta condition via the Kutta-Joukowski theorem) are shown to be good for low Mach number cases at moderate angles of attack.

Comparisons are drawn with traditional Panel methods and the presented technique is found to be easier to implement in the cases considered, however, there is a comparative loss in accuracy for pressure coefficient predictions.

CONTENTS.

1. INTRODUCTION.

This report details the aims, methods and results of a 14 week project conducted at The International Centre For Numerical Methods In Engineering (C.I.M.N.E.), Barcelona, as part of the final year, Master of Engineering (M.Eng) course of The Aeronautics Department of Imperial College London.

The broad aims of the project were to develop a description of the flow around an aerofoil in two dimensions, using the quasi-harmonic potential equation (Laplace) and further, to investigate possible methods to improve the solutions obtained, in terms of speed, cost and efficiency.

The attractive quality of Laplace's equation is that it is linear and thus potential fields, satisfying this equation, are superposable, allowing great flexibility in the construction of the overall solution. However, Laplace's equation is inviscid and isentropic (irrotational) which restricts its domain of physical relevance to low Mach number cases. Although the applicability of the method is restricted, in these limited cases, potential solutions have been shown to give excellent results, as compared with experiment.

The inviscid nature of the Laplace equation demands that any solution derived using this equation will not, directly, describe the forces experienced by a body in a real flow. Instead, various steady, irrotational (continuous) flow fields will need to be synthesised to describe the real flow. In this report, the flow about an aerofoil is described, together with the manner in which the viscosity, by causing the fluid to flow smoothly past the sharp trailing edge, is responsible for generating a circulation which, in turn, is directly proportional to the lift. Once the condition of smooth flow at the trailing edge is imposed (Kutta condition), the methods of inviscid flow analysis enable calculation of the aerodynamic characteristics of the aerofoil. Indeed, once the flow field is known, Bernoulli's equation can be used to calculate the pressure distribution on the surface of the body; the forces and moments acting then follow from integration of the pressures and moments over the surface.

In this report, the Finite Element Method is used to calculate the "non-lifting" potential field around an aerofoil and then a circulation is imposed (at the quarter chord point) to yield the Kutta condition at the trailing edge. An overview of the solution technique is as follows:

1). The "non-lifting" potential and velocity fields are calculated by solving Laplace's equation by the Finite Element Method. Dirichlet type (imposed value) boundary conditions are applied at the edge of the domain to impose the oncoming flow conditions and Neumann, or natural, boundary conditions, of no flow normal to the body surface, are applied at the aerofoil surface (see later section on Boundary Conditions).

2). The Kutta condition is then imposed at the trailing edge by calculating the required circulation to move the rear stagnation point to the trailing edge. The superposition of the flow fields, of (1) and the circulation, violates the required boundary conditions, generating flow through the surface of the aerofoil and yielding incorrect farfield flow conditions.

3). The desired boundary conditions are re-imposed by superposing an additional flow field (given by the solution of the Laplace's equation using the Finite Element Method as before) consisting of exactly the opposite normal velocities at the aerofoil surface, as yielded by the circulation, together with the necessary farfield velocities to reobtain the original oncoming flow.

However, at the end of step (3), the re-imposition of the required boundary conditions tends to move the rear separation point away from the trailing edge, so the processes (2) and (3) are repeated iteratively until convergence.

A modified version of an existing program for the solution of the quasi-harmonic equation (POISS2D) was used as the basis of the potential solver, with auxiliary programs being written to generate the appropriate boundary conditions and circulatory flow fields.

The completed programs were run on the Convex 120 "supercomputer" at C.I.M.N.E., and the generated data was then analysed graphically and by use of the FLAVIA graphical post-processor package, run on a Silicon Graphics Workstation.

2. THEORY.

In this section, it is sought to develop the theoretical basis for the solution techniques employed during this project.

2.1. Velocity Potential.

It may be shown (see Reference 1.) that the angular velocity of a fluid element in three-dimensional space is given by:

$$\omega = \frac{1}{2}\left[\left(\frac{\partial w}{\partial y} - \frac{\partial v}{\partial z}\right)\mathbf{i} + \left(\frac{\partial u}{\partial z} - \frac{\partial w}{\partial x}\right)\mathbf{j} + \left(\frac{\partial v}{\partial x} - \frac{\partial u}{\partial y}\right)\mathbf{k}\right] \qquad 2.1.(1).$$

This expresses the angular velocity of a fluid element in terms of the velocity field, or more precisely, in terms of the derivatives of the velocity field.

The angular velocity of a fluid element plays an important role in aerodynamics and it has been proved useful to define a new quantity, vorticity, which is simply twice the angular velocity. Therefore, define the vorticity as:

$$\xi \equiv 2\omega$$

$$\xi = \left(\frac{\partial w}{\partial y} - \frac{\partial v}{\partial z}\right)\mathbf{i} + \left(\frac{\partial u}{\partial z} - \frac{\partial w}{\partial x}\right)\mathbf{j} + \left(\frac{\partial v}{\partial x} - \frac{\partial u}{\partial y}\right)\mathbf{k} \qquad 2.1.(2).$$

$$\xi = \nabla \times V$$

It is thus seen that, in a velocity field, the vorticity is equal to the curl of the velocity. This defines that:

1). If the vorticity is non-zero throughout the flow field, then the flow is termed rotational and implies that the fluid elements have a finite angular velocity.

2). If the vorticity is zero at every point in the flow then the flow is termed irrotational and implies that the fluid elements have no angular velocity, rather, their motion through space is pure translation.

If the flow is two dimensional then:

$$\xi = \xi_z \mathrm{k} = \left(\frac{\partial v}{\partial x} - \frac{\partial u}{\partial y} \right) \mathbf{k} \qquad 2.1.(3).$$

If the flow is irrotational then this demands that:

$$\frac{\partial v}{\partial x} - \frac{\partial u}{\partial y} = 0 \qquad 2.1.(4).$$

In irrotational flow, it has been shown that:

$$\xi = \nabla \times V = 0 \qquad 2.1.(5).$$

Consider, then, the following vector identity: if ϕ is a scalar function then:

$$\nabla \times (\nabla \phi) = 0 \qquad 2.1.(6).$$

This states that the curl of a scalar function is identically zero. Comparing the previous two equations yields:

$$V = \nabla \phi \qquad 2.1.(7).$$

Equation 2.1.(7). states that for an irrotational flow, there exists a scalar function, ϕ, such that the velocity is given by the gradient of ϕ. ϕ is denoted as the velocity potential and is a function of spatial coordinates. From the definition of the gradient in Cartesian coordinates, equation 2.1.(6). shows that:

$$u\mathbf{i} + v\mathbf{j} + w\mathrm{k} = \frac{\partial \phi}{\partial x}\mathbf{i} + \frac{\partial \phi}{\partial y}\mathbf{j} + \frac{\partial \phi}{\partial z}\mathbf{k} \qquad 2.1.(8).$$

The coefficients of like unit vectors must be the same on both sides of the previous equation. Thus, in Cartesian coordinates:

$$u = \frac{\partial \phi}{\partial x} \qquad v = \frac{\partial \phi}{\partial y} \qquad w = \frac{\partial \phi}{\partial z} \qquad 2.1.(9).$$

The velocity potential is analogous to the stream function in the sense that the derivatives of both yield the flow-field velocities and indeed, the stream function can also be shown to satisfy Laplace's equation. It should be noted, however, that their respective definitions apply different restrictions on their use:

1). Flow-field velocities are obtained by differentiating the velocity potential in the same direction as the velocities, whereas the stream function is differentiated normal to the velocity direction.

2). The potential function is defined for irrotational flow only. In contrast, the stream function may be defined in both rotational and irrotational flow.

3). The velocity potential applies to three dimensional flow, whereas the stream function may only be defined for two dimensional flows.

When a flow is irrotational, allowing a velocity potential to be defined, there is a tremendous simplification. Instead of dealing with the velocity components as unknowns, hence requiring three equations to describe them, the velocity potential can be defined as a single unknown, thereby requiring only one equation to describe the flow-field. Once the potential field is known, the velocity field can be deduced from equation 2.1.(9). For this reason, the potential function was chosen as the operating variable for the considered application.

2.2. Laplace's Equation.

For the definition of Laplace's equation it is necessary to apply one further restriction, that of incompressibility.

Consider the physical definition of incompressible flow, namely ρ = constant. Since ρ is the mass per unit volume and ρ is constant, then a fluid element of fixed mass moving through an incompressible flow field must also have a fixed constant volume. Now, the divergence of the velocity is physically the time rate of change of the volume of a moving fluid element per unit volume. However, as previously stated, the volume of a fluid element is constant in incompressible flow. Thus, for an incompressible flow:

$$\nabla \cdot V = 0 \qquad 2.2.(1).$$

The fact that the divergence of the velocity is zero for an incompressible flow can also be shown directly from the continuity equation, that is:

$$\frac{\partial \rho}{\partial t} + \nabla \cdot \rho V = 0$$

$$0 + \rho \nabla \cdot V = 0 \qquad 2.2.(2).$$

$$\nabla \cdot V = 0$$

Which is the same result as before.

Now, the velocity potential is defined by equation 2.1.(7)., substituting into equation 2.2.(1). gives for a flow which is both irrotational and incompressible that:

$$\nabla^2 \phi = 0 \qquad 2.2.(3).$$

This equation is known as Laplace's equation which has wide ranging significance in many fields of physics and, as such, is one of the most famous and extensively studied equations in mathematical physics.

From the previous discussions, the following obvious, yet important, conclusions may be drawn:

1). Any irrotational, incompressible flow has a velocity potential that satisfies Laplace's equation.

2). Conversely, any solution of Laplace's equation represents the velocity potential for an incompressible, irrotational flow.

It is also noted that Laplace's equation is a second order linear partial differential equation. The fact that it is linear is of particular importance, since the sum of any particular solutions of a linear differential equation, is also a solution of the equation. Thus, since irrotational, incompressible flow is governed by Laplace's equation and Laplace's equation is seen to be linear, then a complicated flow pattern for an irrotational, incompressible flow can be synthesised by adding together a number of constituent (elementary) flows which themselves are both irrotational and incompressible. This is the underlying strategy for the solution of potential flow problems.

The fact that an infinite variety of irrotational, incompressible flow fields may be described by Laplace's equation, indicates the importance of the boundary conditions that, ultimately, distinguish one flow from the next. The required boundary conditions will be discussed generally in the following section and will be treated more fully later in this report.

Consider the external aerodynamic flow over a stationary body, such as the aerofoil sketched below:

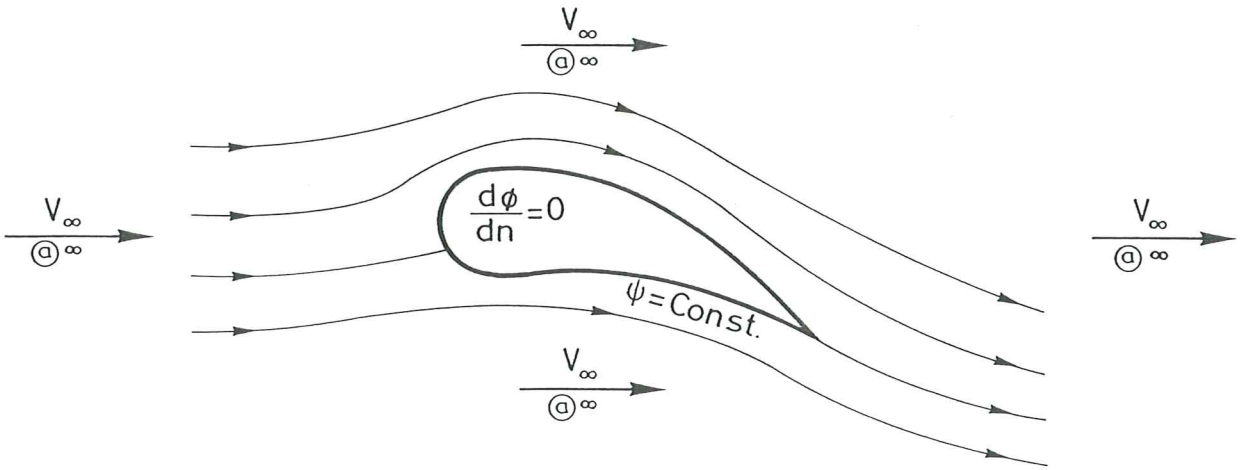

Fig. 2.2.i. (Aerofoil with boundary conditions)

In the above diagram, the flow is bounded by, firstly the freestream flow which is, theoretically, at an infinite distance away from the body and secondly, the surface of the body itself. Thus there are two sets of boundary conditions to apply.

Far away from the body (tending to infinity) in all directions, the flow approaches the uniform freestream conditions. Thus, the outer boundary conditions are that the velocities are the same as the velocities of the freestream at infinity. It must be remembered that this boundary condition is only true at an infinite distance from the body, however, in practice, this means "a long way" (nominally 10 chord lengths) away from the body.

If the surface of the body is solid, then it is impossible for the flow to penetrate the surface. Instead, if the flow is viscous, the effect of friction between the fluid and the boundary is to create zero velocity at the boundary (the "no slip" condition). Such viscid flows are outside the scope of this report. In contrast, for inviscid flows, the velocity at the surface can be finite, but, since the flow cannot penetrate the surface, the velocity vector must be a tangent to the surface ("wall tangency" condition). If the flow is tangential to the surface, then the component of the velocity normal to the surface, must be zero. Let n be a unit vector normal to the surface, then the body boundary condition is:

$$V \cdot n = (\nabla \phi) \cdot n = 0$$
$$\frac{\partial \phi}{\partial n} = 0 \qquad \text{2.2.(4).}$$

With the imposition of the above boundary conditions, the specifics of the required flow may be chosen.

2.3. Vortex Flow.

Consider a flow in which all the streamlines are concentric circles about a given point. Moreover, let the velocity along any given circular streamline be constant and let the velocity vary from one streamline to the next inversely with distance from the common centre. Such a flow is called vortex flow as is shown graphically below:

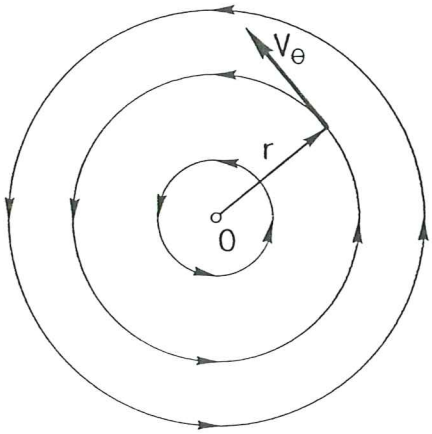

Fig 2.3.1. Vortex flow.

In such a flow, there is no velocity component in the radial direction and the velocity in the tangential direction will be given as a constant divided by the radius. It may be easily demonstrated, that vortex flow is a physically possible incompressible flow ie. the divergence of the velocity is zero everywhere. Also vortex flow is irrotational ie. the curl of the velocity is zero at every point except the origin (where there is a singularity).

Thus, from the definition of vortex flow:

$$V_\theta = \frac{\text{const}}{r} = \frac{C}{r} \qquad \text{2.3.(1).}$$

To evaluate the constant C, take the circulation around a given circular streamline of radius r.

$$V_\theta = -\frac{\Gamma}{2\pi r}$$
$$C = -\frac{\Gamma}{2\pi} \qquad 2.3.(2).$$

Therefore, for vortex flow, this demonstrates that the circulation taken about all streamlines is the same value, namely $\Gamma = 2\pi C$. By convention, Γ is called the strength of the vortex flow and the above equations give the velocity field for a vortex flow of strength Γ. The velocity components in the Cartesian directions may also easily be defined:

$$u = -\frac{\Gamma}{2\pi}\left(\frac{y}{x^2+y^2}\right) \qquad v = \frac{\Gamma}{2\pi}\left(\frac{x}{x^2+y^2}\right) \qquad 2.3.(3).$$

As earlier stated, the vortex flow is irrotational everywhere except at the origin. At the origin, the vorticity tends to infinity. Therefore, the origin is a singular point in the flow field. Hence, the singularity itself may be interpreted as a point vortex which includes about it the circular vortex flow.

The velocity potential for vortex flow may be obtained as follows:

$$\frac{\partial \phi}{\partial r} = V_r = 0$$
$$\frac{1}{r}\frac{\partial \phi}{\partial \theta} = V_\theta = -\frac{\Gamma}{2\pi r} \qquad 2.3.(4).$$
$$\phi = -\frac{\Gamma}{2\pi}\theta$$

2.4. The Kutta-Joukowski Theorem.

It may be shown that any lifting body has associated with it a circulatory field (see reference 2.). For example, consider the incompressible flow over the aerofoil depicted below. Let curve A be any curve that encloses the aerofoil. Let B be any curve that does not enclose the aerofoil. If the aerofoil is producing lift, then the velocity field around the aerofoil will be such that the line integral of velocity around A will be finite, whereas the integral around B will be zero. This demands that the circulation around A will also be finite.

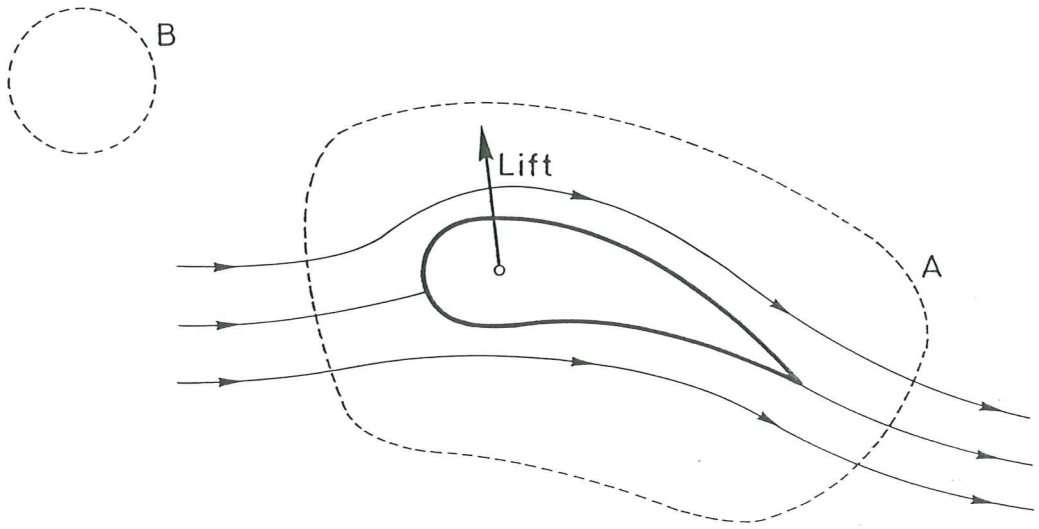

$$\Gamma \equiv \oint_A V \cdot ds \qquad 2.4.(1).$$

In turn, the lift per unit span, L', on the aerofoil will be given by the Kutta-Joukowski theorem, which states that:

$$L' = -\rho_\infty V_\infty \Gamma \qquad 2.4.(2).$$

This result emphasises the importance of the concept of circulation. The Kutta-Joukowski theorem thus states that the lift per unit span on a two dimensional body is directly proportional to the circulation around the body. The general derivation of equation 2.4.(2) has been omitted from this report, but a full treatment may be found in reference 2.

From the above, it can be seen that lifting flow over an aerofoil, such as the one depicted above, may be described by the superposition of elementary flows and further, that such a flow may be deemed irrotational at all points in the flow, except at the origin.

The approach that has been discussed above, forms the basis for the circulation theory of lift that has been utilised in this project. It should be remembered, however, that this is only an alternative way of thinking about the generation of lift on an aerodynamic body. It should be kept in mind that the physical sources of the aerodynamic force on a body are the pressures and the shear stress distributions exerted on the surface of the body. Thus the Kutta-Joukowski theorem is just an alternate way of expressing the consequences of the surface pressure distribution; it is a mathematical expression that is consistent with the tools that have been devised to analyse inviscid, incompressible flow. It is, however, generally much easier to calculate the circulation about a body than to calculate the detailed surface pressure distribution, therein lies the power of this theory.

2.5. The Kutta Condition.

The theory that has been discussed in the previous sections is still incomplete. For a given aerofoil, in a given flow, at a given angle of attack, there are an infinite number of possible values of circulation which give mathematically possible results. However, a given aerofoil, in a given flow, at a given angle of attack, yields only one value of lift. Thus, it is seen that nature "knows" how to choose one particular value of circulation in one particular set of conditions and in analysis, an extra condition is required to precisely define the circulation. This condition is the Kutta condition.

As previously stated, the Kutta-Joukowski theorem states that the force experienced by a body in a uniform stream is equal to the product of the fluid density, stream velocity and circulation, and acts in a direction perpendicular to the free stream. It has also been shown that one and only one irrotational flow can be found that satisfies the boundary conditions at infinity and the body, provided that the circulation is specified.

The irrotational inviscid theory thus far developed, indicates that the geometry of the body and the freestream velocity do not uniquely define the circulation and in order to find the forces acting on the body, it has been shown that, it is necessary to know the exact value of the circulation.

The above discussion applies to an inviscid flow, but in a viscous fluid (however small the viscosity), the circulation is fixed by the imposition of an empirical observation. Experiments show that when a body with a sharp trailing edge is set in motion, the action of the fluid viscosity causes the flow over the upper and lower surfaces to merge smoothly at the trailing edge. This circumstance, which fixes the magnitude of the circulation around the body is known as the Kutta condition which can be stated as follows:

"A body with a sharp trailing edge in motion through a fluid creates about itself a circulation of sufficient strength to hold the rear stagnation point at the trailing edge." (reference 3.)

The flow around an aerofoil at an angle of attack in an inviscid flow develops no circulation and the rear stagnation point occurs on the upper surface of the aerofoil; the streamlines of such a flow is shown schematically below:

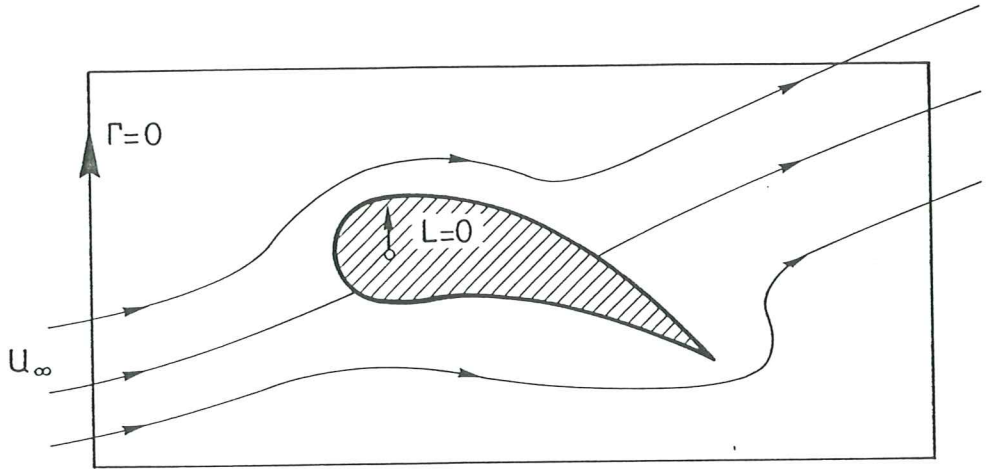

Fig.(1). Inviscid flow around an aerofoil.

In viscous flow, the aerofoil creates around itself a circulation which fixes the rear stagnation point at the trailing edge. The smooth merging of the upper and lower flows at the trailing edge is shown schematically below:

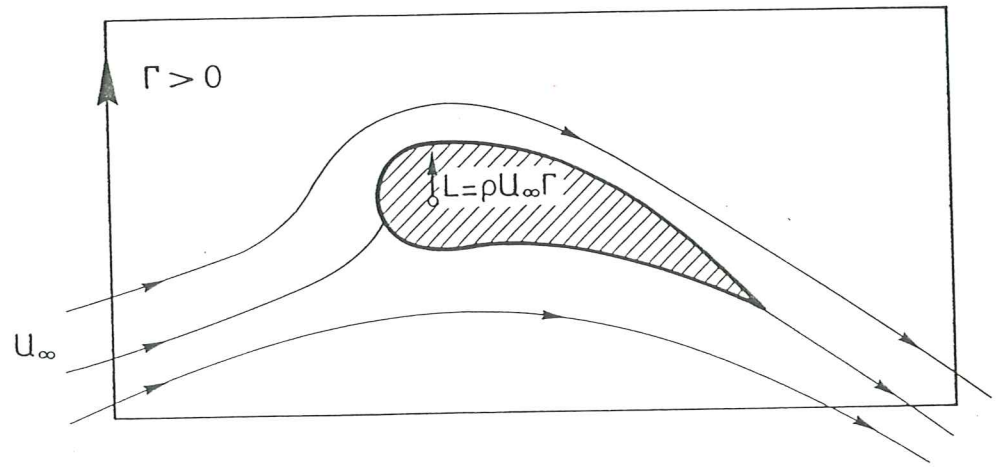

Fig.(2). Viscous flow around an aerofoil.

With the above discussion, the theoretical basis for the analysis undertaken has been developed.

2.6. The Finite Element Method.

As stated in the introduction, the Finite Element Method was used to solve Laplace's equation and derive the uniquely specified potential flow (from the geometry and boundary conditions). Pursuant to this, presented here is a brief overview of the well known theory behind the Finite Element Method, with a particular bias toward the treated problem. A more rigorous treatment of the Finite Element Method may be found in reference 4.

Laplace's equation is a specific form of the quasi-harmonic equation in two-dimensions. For generality, first consider the full equation:

$$\frac{\partial}{\partial x}\left(K_x \frac{\partial \phi}{\partial x}\right) + \frac{\partial}{\partial y}\left(K_y \frac{\partial \phi}{\partial y}\right) + Q = 0 \qquad 2.6.(1).$$

In which ϕ is the unknown function (in this case the velocity potential) and K_x, K_y and Q are material parameters which may be functions of x and y. A number of different field problems may be described using this general equation, but for the application currently being considered the following is noted:

$K_x = K_y = 1$
$Q = 0$

This yields Laplace's equation.

For this equation, there are two main types of boundary condition which are of interest. With reference to 2.6.(1)., it may be required that:

a). The value of the unknown to be specified at nodal points on the boundary, ie.:

$$\phi = \phi_p \qquad 2.6.(2).$$

This is termed, mathematically, as the Dirichlet boundary condition and is the boundary condition that is prescribed, in this application, at the farfield boundary (see Methodology and Implementation section.).

b). That a boundary "loading" exists of the form:

$$K_x \frac{\partial \phi}{\partial x} L_x + K_y \frac{\partial \phi}{\partial y} L_y + q + \alpha(\phi - \phi_a) = 0 \qquad 2.6.(3).$$

In which q, α and ϕ_a are constants and L_x and L_y are the direction cosines between the outward normal, n, and the x and y axes respectively. This is termed the Cauchy boundary condition. In the case of flow about an aerofoil boundary conditions of both types (a) and (b) exist in the problem and the problem is termed "*mixed*".

The physical significance of the second boundary condition is not easily seen and thus, its' significance will be illustrated with regard to the present problem with $K_x = K_y = 1$. In this case the boundary condition (b) reduces to:

$$\frac{\partial \phi}{\partial n} + q + \alpha(\phi - \phi_a) = 0 \qquad 2.6.(4).a.$$

Where $d\phi/dn$ is the velocity normal to the surface at the point of consideration. By taking appropriate values of q and α, well established physical boundary conditions can be derived:

(i): $q = \alpha = 0$, then:

$$\frac{\partial \phi}{\partial n} = 0 \qquad 2.6.(4).b.$$

This implies that the velocity normal to the boundary is zero. In other words, this implies that the surface is solid. This condition is termed the Neumann or natural boundary condition.

(ii): $\alpha = 0$, then:

$$\frac{\partial \phi}{\partial n} = -q \qquad 2.6.(4).c.$$

This is the flux boundary condition, which states that a specified amount of fluid, q, flows into the body per unit area of surface.

The previous two boundary conditions are applied in the execution of the finite element technique for the considered problem. For completeness, however, a third, unused, physical boundary condition will be given.

(iii): q = 0. then:

$$\frac{\partial \phi}{\partial n} = -\alpha(\phi - \phi_a) \qquad 2.6.(4).d.$$

This states that the flow of fluid from any point of the surface is directly proportional to the difference in velocity potential between the point in question and the prescribed potential, ϕ_a. This is termed the convection boundary condition.

2.6.a. The Galerkin Method.

In order to reduce this continuum problem to a finite set of unknowns, some discretisation procedure must be undertaken. To do this the Galerkin weighted residual process will be employed to set up the necessary "stiffness" equations. Define the errors associated with solving 2.6.(1). and 2.6.(3). by e_A and e_S respectively, so that:

$$\begin{aligned} e_A &= \frac{\partial}{\partial x}\left(K_x\frac{\partial\phi}{\partial x}\right)+\frac{\partial}{\partial y}\left(K_y\frac{\partial\phi}{\partial y}\right)+Q \\ e_S &= K_x\frac{\partial\phi}{\partial x}L_x+K_y\frac{\partial\phi}{\partial y}L_y+q+\alpha(\phi-\phi_a) \end{aligned} \qquad \text{2.6.(5).}$$

Since boundary condition type (a) of 2.6.(2). is directly satisfied by the prescription of ϕ, there is no error associated with this term. In the weighted residual approach, it is sought to minimise, in some global manner, the residuals e_A and e_S weighted by some suitable weighting functions w_A and w_S. In particular, it is required that:

$$\int_A e_A w_A dA+\int_{S_B} e_S w_S dS=0 \qquad \text{2.6.(6).}$$

Where S_B denotes the part of the boundary on which boundary condition type (b) applies. Substituting from 2.6.(5). into 2.6.(6). gives:

$$\begin{aligned} &\int_A\left[\frac{\partial}{\partial x}\left(K_x\frac{\partial\phi}{\partial x}\right)+\frac{\partial}{\partial y}\left(K_y\frac{\partial\phi}{\partial y}\right)+Q\right]w_A dA \\ &+\int_{S_B}\left[K_x\frac{\partial\phi}{\partial x}L_x+K_y\frac{\partial\phi}{\partial y}L_y+q+\alpha(\phi-\phi_a)\right]w_s dS=0 \end{aligned} \qquad \text{2.6.(7).}$$

Now, Green's theorem relates the integrals of quantities over a region A and over its' boundary S, as follows:

$$\int_A\left(\frac{\partial C}{\partial x}\frac{\partial D}{\partial x}+C\frac{\partial^2 D}{\partial x^2}\right)dA=\int_S C\frac{\partial D}{\partial x}L_x dS \qquad \text{2.6.(8).}$$

In which C and D are arbitrary scalar functions and a similar expression holds for the y variable. Applying 2.6.(8). to the second order derivatives in 2.6.(7). results in:

$$\begin{aligned} &\int_S\left[K_x\frac{\partial\phi}{\partial x}L_x+K_y\frac{\partial\phi}{\partial y}L_y\right]w_A dS \\ &-\int_A\left[K_x\frac{\partial w_A}{\partial x}\frac{\partial\phi}{\partial x}+K_y\frac{\partial w_A}{\partial y}\frac{\partial\phi}{\partial y}-Qw_A\right]dA \\ &+\int_{S_B}\left[K_x\frac{\partial\phi}{\partial x}L_x+K_y\frac{\partial\phi}{\partial y}L_y+q+\alpha(\phi-\phi_a)\right]w_S dS=0 \end{aligned} \qquad \text{2.6.(9).}$$

At this stage, it is chosen that $w_S = -w_A$ (= w, say) so that 2.6.(9). becomes, on use of 2.6.(3).:

$$\int_{S_A}\left[K_x\frac{\partial\phi}{\partial x}L_x + K_y\frac{\partial\phi}{\partial y}L_y\right]w\ dS - \int_{S_B}[q+\alpha(\phi-\phi_a)]w\ dS - \int_A\left[K_x\frac{\partial w}{\partial x}\frac{\partial\phi}{\partial x} + K_y\frac{\partial w}{\partial y}\frac{\partial\phi}{\partial y} - wQ\right]dA = 0 \qquad \text{2.6.(10).}$$

Where S_A is the part of the boundary on which boundary condition type (a) applies.

It is noted that at each point on the boundary either boundary condition type (a) or boundary condition type (b) must be specified. Note that if no conditions are specified on a portion of the boundary, then condition type (b) with $q = \alpha = 0$ is automatically implied.

2.6.b. Finite Element Discretisation.

If finite element discretisation is now adopted, then the unknown function ϕ, may be approximated as:

$$\phi = \sum_{i=1}^{n} N_i\phi_i \qquad \text{2.6.(11).}$$

In which n is the total number of nodes, N_i are the global shape functions and ϕ_i are the nodal values of ϕ. In the Galerkin process, the number of weighting functions must equal the total number of nodal unknown values. The weighting functions corresponding to node i, w_i, can then be conveniently chosen so that $w_i = N_i$.

Substituting for f from 2.6.(11). into 2.6.(10). and setting $w_i = N_i$ gives:

$$X_i - \int_{S_B} N_i\left[q - \alpha\phi_a + \alpha\sum_{j=1}^{n} N_j\phi_j\right]dS - \int_A\left[\sum_{j=1}^{n}\left[K_x\frac{\partial N_i}{\partial x}\frac{\partial N_j}{\partial x} + K_y\frac{\partial N_i}{\partial y}\frac{\partial N_j}{\partial y}\right]\phi_j - N_iQ\right]dA = 0 \qquad \text{2.6.(12).}$$

with:

$$X_i = \int_{S_A} N_i\sum_{j=1}^{n}\left[K_x\frac{\partial N_j}{\partial x}L_x + K_y\frac{\partial N_j}{\partial y}L_y\right]dS\phi_j \qquad \text{2.6.(13).}$$

Where A is the area of the domain of interest and S_A and S_B are the parts of the boundary on which boundary conditions type (a) and (b) are respectively imposed. There are i = 1,n equations

of this form. Rearranging gives:

$$\sum_{j=1}^{n} \left\{ \int_A \left[K_x \frac{\partial N_i}{\partial x}\frac{\partial N_j}{\partial x} + K_y \frac{\partial N_i}{\partial y}\frac{\partial N_j}{\partial y} \right] dA + \alpha \int_{S_B} N_i N_j dS \right\} \phi_j = \int_A Q N_i dA - \int_{S_B} (q - \alpha\phi_a) N_i dS + X_i \qquad 2.6.(14).$$

Which can be expressed in matrix form as:

$$\mathbf{K}\phi = \mathbf{f} \qquad 2.6.(15).$$

In which, the global "stiffness" and "force" vector are:

$$k_{ij} = \int_A \left[K_x \frac{\partial N_i}{\partial x}\frac{\partial N_j}{\partial x} + K_y \frac{\partial N_i}{\partial y} \right] dA + \alpha \int_{S_B} N_i N_j dS \qquad 2.6.(16).$$

and

$$f_i = \int_A Q N_i dA - \int_{S_B} (q - \alpha\phi_a) N_i dS + X_i \qquad 2.6.(17).$$

The explicit form of X_i need not be written in 2.6.(17). since this term is never input as an applied load. From 2.6.(13). it is recalled that X_i represents a loading on the part S_A of the boundary. However, according to 2.6.(2). the value of the variable, ϕ, is prescribed everywhere along the boundary region S_A. Hence, the term X_i represents the "force" reaction at each nodal point associated with the prescribed "displacement" values along boundary S_A.

In order to discretise the domain, a mesh was generated of general three noded triangular elements (see section on mesh generation). In the following, a brief overview is given of the method of calculating the "stiffness" and "load" terms. First the theory of right triangular elements will be discussed (as defined in natural coordinates) and secondly, how these local right triangular elements may be transformed to triangular elements of general shape, in global coordinates.

Consider an isoparametric formulation for a n node triangle or quadrilateral element. The geometry of such an element may be expressed using the nodal coordinates $x_i^{(e)}$ and $y_i^{(e)}$ and the shape functions defined in natural coordinates, $N_i^{(e)}(\xi,\eta)$. Thus at any point within the element the x and y coordinates may be obtained from the expressions:

$$x(\xi,\eta) = \sum_{i=1}^{n} N_i^{(e)} x_i^{(e)}$$
$$y(\xi,\eta) = \sum_{i=1}^{n} N_i^{(e)} y_i^{(e)} \qquad 2.6.(18).$$

The Cartesian derivative of any function, f, is defined over the element using the expression:

$$f(\xi,\eta) = \sum_{i=1}^{n} N_i^{(e)} f_i^{(e)} \qquad 2.6.(19).$$

Where $f_i^{(e)}$ is the value of f at node i and may be obtained by using the chain rule of integration:

$$\frac{\partial f}{\partial x} = \frac{\partial f}{\partial \xi}\cdot\frac{\partial \xi}{\partial x} + \frac{\partial f}{\partial \eta}\cdot\frac{\partial \eta}{\partial x}$$
$$\frac{\partial f}{\partial y} = \frac{\partial f}{\partial \xi}\cdot\frac{\partial \xi}{\partial y} + \frac{\partial f}{\partial \eta}\cdot\frac{\partial \eta}{\partial y} \qquad 2.6.(20).$$

Where $df/d\xi$ and $df/d\eta$ are evaluated as:

$$\frac{\partial f}{\partial \xi} = \sum_{i=1}^{n} \frac{\partial N_i^{(e)}}{\partial \xi}\cdot f_i^{(e)}$$
$$\frac{\partial f}{\partial \eta} = \sum_{i=1}^{n} \frac{\partial N_i^{(e)}}{\partial \eta}\cdot f_i^{(e)} \qquad 2.6.(21).$$

The terms $d\xi/dx$, $d\eta/dx$, $d\xi/dy$ and $d\eta/dy$ can be obtained using the following procedure. First we evaluate the matrix:

$$\mathbf{J}^{(e)} = \begin{bmatrix} \frac{\partial x}{\partial \xi} & \frac{\partial y}{\partial \xi} \\ \frac{\partial x}{\partial \eta} & \frac{\partial y}{\partial \eta} \end{bmatrix} \qquad 2.6.(22).$$

Which is termed the Jacobian matrix. The inverse of the Jacobian is then evaluated using:

$$[\mathbf{J}^{(e)}]^{-1} = \frac{1}{\det \mathbf{J}^{(e)}} \begin{bmatrix} \frac{\partial y}{\partial \eta} & -\frac{\partial y}{\partial \xi} \\ -\frac{\partial x}{\partial \eta} & \frac{\partial x}{\partial \xi} \end{bmatrix} \qquad 2.6.(23).$$

Note that an elemental area of the element is given by:

$$dx\ dy = \det\mathbf{J}^{(e)} d\xi d\eta \qquad 2.6.(24).$$

For the three node isoparametric element, the element is C(0) continuous and has the following shape functions and derivatives:

$$\begin{aligned} N_1^{(e)} &= 1 - \xi - \eta & \frac{\partial N_1^{(e)}}{\partial \xi} &= -1 & \frac{\partial N_1^{(e)}}{\partial \eta} &= -1 \\ N_2^{(e)} &= \xi & \frac{\partial N_2^{(e)}}{\partial \xi} &= 1 & \frac{\partial N_2^{(e)}}{\partial \eta} &= 0 \\ N_3^{(e)} &= \eta & \frac{\partial N_3^{(e)}}{\partial \xi} &= 0 & \frac{\partial N_3^{(e)}}{\partial \eta} &= 1 \end{aligned} \qquad 2.6.(25).$$

Note that now it is possible to represent any triangular shape which has straight sides, as the following diagram shows:

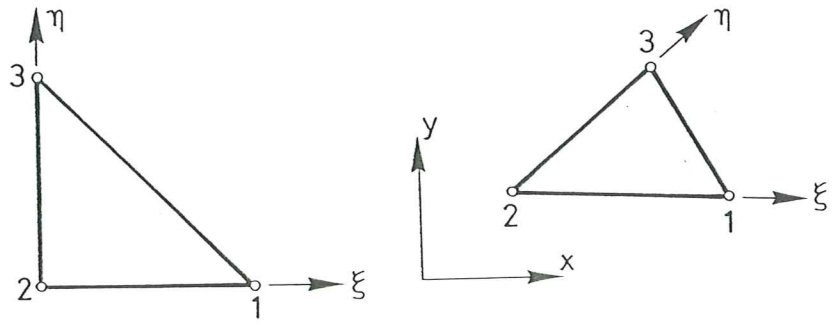

Local definition Global definition

For clarity, adopt the following notation:

$$\begin{aligned} b_1 &= y_2^{(e)} - y_3^{(e)} & c_1 &= x_3^{(e)} - x_2^{(e)} \\ b_2 &= y_3^{(e)} - y_1^{(e)} & c_2 &= x_1^{(e)} - x_3^{(e)} \\ b_3 &= y_1^{(e)} - y_2^{(e)} & c_3 &= x_2^{(e)} - x_1^{(e)} \end{aligned} \qquad 2.6.(26).$$

Then the Jacobian can be written as:

$$\mathbf{J}^{(e)} = \begin{bmatrix} c_3 & -b_3 \\ -c_2 & b_2 \end{bmatrix} \qquad 2.6.(27).$$

The inverse of the Jacobian is then:

$$[\mathbf{J}^{(e)}]^{-1} = \begin{bmatrix} \frac{\partial \xi}{\partial x} & \frac{\partial \eta}{\partial x} \\ \frac{\partial \xi}{\partial y} & \frac{\partial \eta}{\partial y} \end{bmatrix} = \frac{1}{c_3 b_2 - c_2 b_3} \begin{bmatrix} b_2 & b_3 \\ c_2 & c_3 \end{bmatrix} \qquad 2.6.(28).$$

Since:

$$c_3 b_2 - c_2 b_3 = 2A^{(e)} \qquad 2.6.(29).$$

Where A(e) is the area of the triangle, then the Cartesian shape function derivatives can be obtained from 2.6.(20). and 2.6.(21)., giving:

$$\begin{aligned} \frac{\partial N_1^{(e)}}{\partial x} &= \frac{b_1}{2A^{(e)}} \quad \frac{\partial N_1^{(e)}}{\partial y} = \frac{c_1}{2A^{(e)}} \\ \frac{\partial N_2^{(e)}}{\partial x} &= \frac{b_2}{2A^{(e)}} \quad \frac{\partial N_2^{(e)}}{\partial y} = \frac{c_2}{2A^{(e)}} \\ \frac{\partial N_3^{(e)}}{\partial x} &= \frac{b_3}{2A^{(e)}} \quad \frac{\partial N_3^{(e)}}{\partial y} = \frac{c_3}{2A^{(e)}} \end{aligned} \qquad 2.6.(30).$$

The "stiffness" and "load" matrices of 2.6.(16). and 2.6.(17)., respectively, may now be evaluated (see reference 3.) to construct the desired system 2.6.(15).

3. MESH GENERATION.

In order to apply the Finite Element Method to the solution of Laplace's equation, it was necessary to discretise the physical domain. This required the generation of a mesh which would split the domain down to acceptably sized elements to approximate the physical reality by the Finite Element Method.

There are a wide variety of different techniques available to generate meshes around an aerofoil shape and presented here is a brief overview of the options considered for the method of mesh generation (a more complete overview of meshing and optimisation techniques may be found in reference 5.).

a). Structured Meshes From Partial Differential Equations.

The majority of physical problems may be described in terms of partial differential equations. It has been proved advantageous to generate meshes that have an intimate connection with the properties of the equations that are wished to be solved. These problems fall naturally into 3 main categories; equilibrium problems, such as Laplace's equation which is known as a boundary value problem (the governing equations are elliptic); eigenvalue problems and propagation problems (with hyperbolic or parabolic governing equations).

It may seem inappropriate to suggest that a system of partial differential equations should be solved to form the mesh before solving the real system and indeed, for the present application, this is an inappropriate meshing method. However, the approach has been proved viable and has been used successfully for a range of applications.

b). Conformal and Orthogonal Mapping.

The methods of conformal mapping are well known in fluid dynamics and it has been seen that these techniques can offer a means of mesh generation. A geometrically complicated domain can be mapped into a simple domain within which a mesh is generated. Inverting the mesh into the physical domain then results in an orthogonal computational mesh in the physical domain.

The drawback of such an approach is that conformal mapping algorithms impose the distribution of mesh points along boundaries and it is not possible to fix point distributions in the interior of the domain. Hence, it is not applicable for apriori mesh point clustering to known features of either the flow or the geometry. However, as a methodology for generating meshes for the solution of potential flow, the orthogonality presents some desirable features.

c). Algebraic Mesh Generating Techniques.

Algebraic mesh generation techniques provide a direct functional description of the transformation between the computational and physical domains. Conformal mapping is an algebraic mesh generation technique, however, a class of mesh generation techniques has grown up to relax the disadvantages of the conformal mapping technique.

d). Unstructured Meshes - The Advancing Front method.

The advancing front technique is one of the most generally applicable mesh generation techniques. It is based on the idea of the simultaneous mesh point generation and connectivity. Given a set of points which defines a geometrical boundary or boundaries and a measure of the local spacing required within the domain, the method extends or advances the boundary connectivity into the field. Mesh points are generated and connected to other local points and in this way the mesh is advanced away from the boundaries. The mesh point density is controlled by the user specified parameters which in the basic form, for a uniform mesh, can be a single value which represents the desired spacing throughout . The nature of the method makes it ideally applicable to the most complicated of shapes and requires the minimum amount of data from the user. For these reasons the advancing front technique was chosen as the method of mesh generation for this project. The two-dimensional unstructured mesh generator (2dumg), written by Dr. Gabriel Bugeda of C.I.M.N.E., was used to generate, first the profile (using B-splines) and then the mesh for N.A.C.A. profile data, supplied by Dr. Fernando Quintana also of C.I.M.N.E.

e). Other Methods.

Many approaches have been developed which seek to take advantage of the properties of both structured and unstructured grid generation techniques. Generally it is desired to create an appropriate local mesh topology. One such approach is the "Multiblock" approach and the reader is pointed towards reference 5. for a more complete treatment of the alternative methods.

4. METHODOLOGY AND IMPLEMENTATION.

With regard to the available facilities, it was decided that the most propitious solution method would be as follows:

a). A program would be written that would solve Laplace's equation in two dimensions, with the ability to handle mixed boundary conditions to generate a potential field.

b). The geometry of the aerofoil and the surrounding domain would then be discretised by use of the 2dumg mesh generation program.

c). When the potential field solver had been run for a given set of boundary conditions. The resulting "non-lifting" potential field would be analysed to establish the required circulation (applied at the theoretical centre of lift, the 1/4 chord point) to yield the rear stagnation point at the trailing edge (the Kutta condition).

d). The velocity field generated by this circulation would then be calculated and added to that of the "non-lifting" potential solver. The resulting field would then be analysed for violations of the desired boundary conditions.

e). The "non-lifting" potential solver would then be re-run with the required boundary conditions to correct the violations caused by the circulation.

f). The subsequent output data would be analysed for any violation of the Kutta condition caused by step (e). The circulation would then be adjusted to re-establish the Kutta condition at the trailing edge and steps (c), (d), (e) and (f) would be repeated until the circulation had converged to within an "acceptable" tolerance.

Once the solution technique had been decided upon, it was first necessary to develop a program which would calculate the potential field created about an aerofoil, with mixed boundary conditions, created by prescribed angle of attack and freestream conditions.

Already in existence at C.I.M.N.E. was a two dimensional solver for Poisson's equation (POISS2D) based on quadrilateral elements, which would run with Dirichlet or Neumann boundary conditions. This program was first converted to run with 3 node triangular C(0) elements (as described in section 2.6.) and then tested against a published case in reference 4.

Once satisfactory results were obtained, the program was further converted to yield the generated elemental and nodal velocities. The elemental velocities can be generated directly from the nodal values of the potential function by use of equations 2.6.(20)., these velocities are however, discontinuous and as such, some approximation had to be made to calculate the nodal values. The simple solution of approximating the nodal velocity to the average of the velocities in all elements to which the node contributes, was chosen. It must be remembered, however, that the nodal values of the velocity are further approximations of an already approximate elemental value and this has proved to be a source of error (see Discussion).

It then became necessary to generate an appropriate mesh around a nominal aerofoil. The N.A.C.A. 0012 aerofoil was chosen, since it has been a popular experimental aerofoil section and, as such, there is a large amount of experimental data available, covering a large range of Reynold's and Mach numbers. Data for the profile section, generated by Dr. Fernando Quintana, was used as input (together with a suitable background mesh) for the 2 dimensional unstructured mesh generation program of Dr. Gabriel Bugeda (2dumg).

The resulting mesh data generated by 2dumg was then converted to an acceptable format for input to the Laplace's equation solver. To do this, a program was written to firstly; reformulate the mesh data to acceptable input for the potential solver and secondly; to calculate the required farfield boundary conditions to impose the correct flow. It is noted at this stage, that no boundary conditions needed to be applied at the aerofoil surface, because, in the absence of a prescribed boundary condition, the Neumann or natural boundary condition of no velocity normal to the aerofoil is applied by default (see section 2.6.). In order to apply the farfield boundary conditions, the following was noted: For any uni-directional freestream with parallel streamlines, the potential function, ϕ, may be defined, analytically, as follows:

$$\phi = V_x.x + V_y.y + \phi_o$$

where: V_x is the freestream velocity in the x direction.

V_y is the freestream velocity in the y direction.

x and y are the Cartesian coordinates of any point in the flow field.

ϕ_o is some "zero" value of the potential function (chosen as 0 in this case).

Thus, once the desired freestream velocity and angle of attack are input to the program, the values of V_x and V_y can be evaluated and thus, the values of f at the outer boundary nodes can then be calculated (their Cartesian positions being known from 2dumg). This allows Dirichlet type boundary conditions to be given as input to the potential solver.

When the potential solver was functioning (after suitable re-dimensioning of the arrays etc.), it was desired to get a graphical representation of the results that had been obtained. To do this, the graphical post-processor package of C.I.M.N.E., FLAVIA, was used. A simple subroutine was appended to the potential solver, which created the required output files of the required format for FLAVIA. Once this was done, FLAVIA proved a great aid to the debugging and development of the working programs.

The FLAVIA output clearly showed the position of the rear stagnation point to be on the upper surface of the aerofoil, for flow with the aerofoil at a positive angle of attack (see Results section). It was then necessary to impose the correct circulation at the 1/4 chord point to give the Kutta condition, but how to calculate this circulation? Various methods were tried, with varying degrees of success and some of them will be sketched out in the following sections.

The simplest way of imposing the Kutta condition is to impose the circulation that will cause the normal (to the local chord) velocity to be zero at the trailing edge. In order to calculate this normal velocity, the calculated nodal velocities at the trailing edge could be used (and indeed were tried) but, as emphasised earlier, these values are false values, especially at the trailing edge, where the changes in elemental values of the velocity are greatest (in directional terms). Thus a circulation calculated on the nodal values of velocity at the trailing edge would yield a falsely high value of required circulation. This method was tried and rejected (it yielded a value of circulation 3 times too great, and the solution did not converge).

A second approach would be to consider the two elements that have two nodes on the aerofoil surface, one of which being the trailing edge node ie. the first and last elements around the aerofoil (starting from the trailing edge). The ultimate effect of the circulation is to cause the velocities in these elements to be of equal values, tangential to the aerofoil surface and both in the direction of the trailing edge. The circulation may be calculated based on correcting these tangential velocities, but this also yields a falsely high value of the circulation, as the effect of re-imposing the aerofoil boundary conditions is difficult to estimate and this has an effect on the tangential velocities.

The third approach and indeed, the one which proved successful, was to calculate the normal velocity between the tangential velocity components at the trailing edge, as shown below:

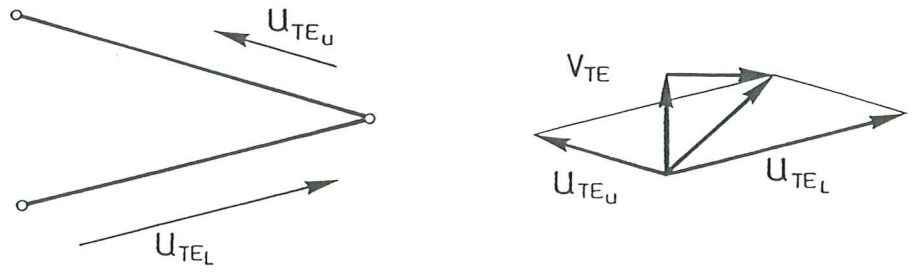

Fig 4.1. Calculation of the vertical velocity component at the trailing edge.

Once the vertical velocity component at the trailing edge is known, the required circulation to give an equal and opposite velocity at the same point is given by the following expression:

$$v = \frac{\Gamma}{2\pi}\left(\frac{x}{x^2+y^2}\right)$$
$$\Gamma = v2\pi\left(\frac{x^2+y^2}{x}\right) \qquad 4.(1).$$

This proved the most efficient method of calculating the desired circulation and indeed, was found to converge rapidly to the desired solution (see Results section).

The velocity field due to the calculated circulation was assessed at each node and in every element (note: the velocities are, here, continuous) by use of equations 2.3.(3).

It is noted that it is difficult to assess the potential field, caused by the circulation, in terms that allow it to be directly added with the initial potential field. This is because, the potential field due to the circulation is a function which spirals up, continually increasing with the angle of sweep around the azimuth, this function is:

$$\phi = \frac{\Gamma}{2\pi}\theta \qquad 4.(2).$$

Thus it is seen, that in a continuous mesh, it is impossible to define the potential field continuously around the azimuth, as there must always be a "jump" in potential value between the value of ϕ at $\theta = 0°$ and $\theta = 360°$. However, the velocity fields that result from a circulation may be calculated continuously for an uncut mesh and due to this, the velocity fields were chosen as the fields to be added.

Associated with the field due to circulation, is the undesired effect of the violation of the required boundary conditions, as the summation of the field yields undesired velocities normal to the aerofoil surface and undesired velocity components at the farfield boundary. These undesired boundary conditions had to be removed to return to the desired boundary conditions of no flow through the aerofoil surface and flow at the outer boundary equal to the freestream flow at infinity.

To create the required corrective field, the original "non-lifting" potential solver was used, however, now there are additional complications with the boundary conditions. At the aerofoil surface, it was required to apply "loads" which exactly counteract the normal components of the velocity that was generated by the circulation. This required some changes to the potential solver program. The theory for this will be given in the following:

For the required boundary conditions:

$$\frac{\partial \phi}{\partial x} - \bar{u} = 0 \qquad 4.(3).a.$$

$$\frac{\partial \phi}{\partial y} - \bar{v} = 0 \qquad 4.(3).b.$$

Multiply 4.(3).a. by the normal in the x direction, n_x, and 4.(3).b. by the normal in the y direction, n_y. Then equating gives:

$$\frac{\partial \phi}{\partial x} n_x + \frac{\partial \phi}{\partial y} n_y - \bar{u} n_x - \bar{v} n_y = 0 \qquad 4.(4).$$

Then a Galerkin error formulation may be written as before (see Theory section):

$$\int_\Omega \omega \left[\frac{\partial^2 \phi}{\partial x^2} + \frac{\partial^2 \phi}{\partial y^2} \right] \partial\Omega + \oint_\Gamma \omega_\Gamma \left[\frac{\partial \phi}{\partial x} n_x + \frac{\partial \phi}{\partial y} n_y - \bar{u} n_x - \bar{v} n_y \right] \partial\Gamma = 0 \qquad 4.(5).$$

Taking the first integral by parts, gives:

$$- \int_\Omega \left(\frac{\partial \omega}{\partial x} \frac{\partial \phi}{\partial x} + \frac{\partial \omega}{\partial y} \frac{\partial \phi}{\partial y} \right) + \oint_\Gamma \omega \left[\frac{\partial \phi}{\partial x} n_x + \frac{\partial \phi}{\partial y} n_y \right] \partial\Gamma + \oint_\Gamma \omega_\Gamma [\quad] \partial\Gamma = 0 \qquad 4.(6).$$

Now w_Γ is arbitrary, therefore set w_Γ = -w and then eliminating gives:

$$\int_\Omega \left(\frac{\partial \omega}{\partial x} \frac{\partial \phi}{\partial x} + \frac{\partial \omega}{\partial y} \frac{\partial \phi}{\partial y} \right) \partial\Omega = \oint_\Gamma \omega \left[\bar{u} n_x + \bar{v} n_y \right] \partial\Gamma \qquad 4.(7).$$

Now, it is noted that in general:

$$U_x.n_x + U_y.n_y = U_n \qquad 4.(8).$$

Where, U_n is the normal velocity and again it is seen that on a boundary where $U_n = 0$, no boundary condition needs to be specified.

For the above equations the same approximations are made as described in 2.6. which ultimately yields the desired:

$$\mathbf{K.a} = \mathbf{f}$$

It is thus seen that a normal velocity is an additional term in the "load" vector and may be evaluated by conducting a line integral over the side of the element that touches the boundary:

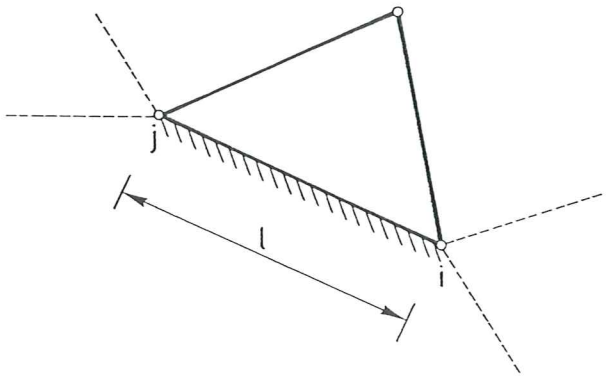

fig 4.2. Boundary Edge Element.

$$\underline{f}_e = \frac{l}{2}\begin{Bmatrix} \bar{u}n_{x_i} & + & \bar{v}n_{y_i} \\ \bar{u}n_{x_i} & + & \bar{v}n_{y_i} \\ & 0 & \end{Bmatrix} \qquad 4.(9).$$

In this manner the, the relevant parts of the "load" vector can be prescribed. It is noted, however, that this prescription relies upon the approximated nodal values of the velocity, which is a source of error.

A routine was then written which calculates the required normals and element lengths and this routine was appended to the program which calculates the circulation, this program then writes a file of boundary conditions for the "non-lifting" potential solver. The potential solver itself was also converted to load the "force" vector with the new input "loads".

With these programs, the iteration process described at the beginning of the chapter was set up and a flowchart for this process may be found in Appendix 1.

In detail, the process is shown below:

1). The first "non-lifting" velocity potential field ($\underline{u}^o$) is obtained by solving Laplace's equation in the domain with the desired boundary conditions ie. no flow through the aerofoil surface and farfield boundary velocities equal to the freestream velocity at infinity). Graphically this is shown below:

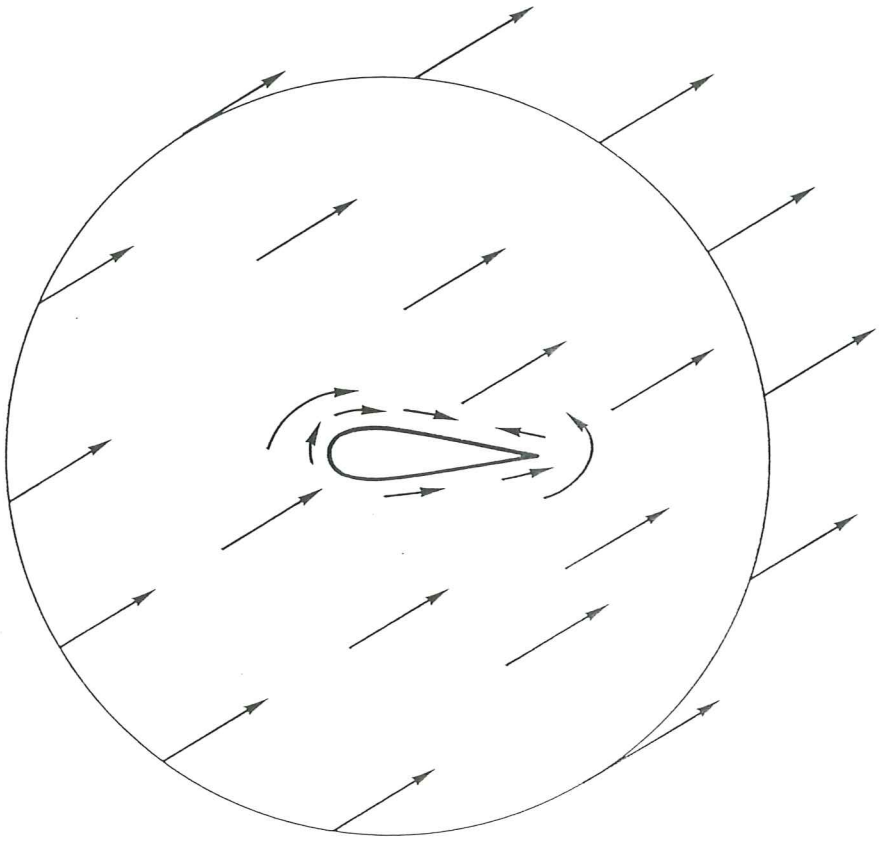

2). The generated velocity field is analysed at the trailing edge to calculate the required circulation to yield the Kutta condition as described previously. The velocity field due to the circulation is then calculated ($\underline{u}^o{}_\Gamma$) yielding the following flow pattern:

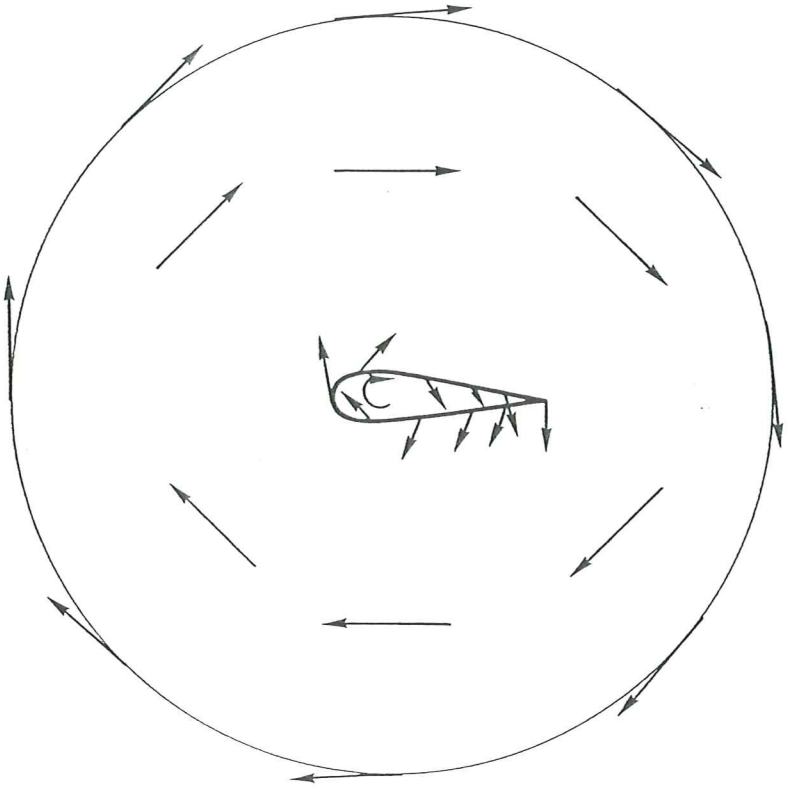

3). The summation of the two previous velocity fields gives a flow field which satisfies the Kutta condition but violates the desired boundary conditions, both at the farfield boundary and at the aerofoil surface. Specifically, the circulation generates a velocity component normal to the aerofoil surface ($\underline{u}^{o}{}_{\Gamma n}$) and undesired components at the farfield boundary ($\underline{u}^{o}{}_{\Gamma B}$). To correct for these undesired components, Laplace's equation is again solved with velocities of $-\underline{u}^{o}{}_{\Gamma n}$ applied at the aerofoil surface and $-\underline{u}^{o}{}_{\Gamma B}$ applied at the farfield boundary. The resulting velocity field is called $\underline{u}^{o}{}_{BC}$.

4). The first trial solution $\underline{u}^{1}$ is then obtained from:

$$\underline{u}^{1} = \underline{u}^{o} + \underline{u}^{o}{}_{\Gamma} + \underline{u}^{o}{}_{BC}$$

The first trial solution field then becomes the subject field for the analysis and steps 2 to 4 are repeated until convergence is achieved.

The resulting velocity field will then be the desired field, that is:

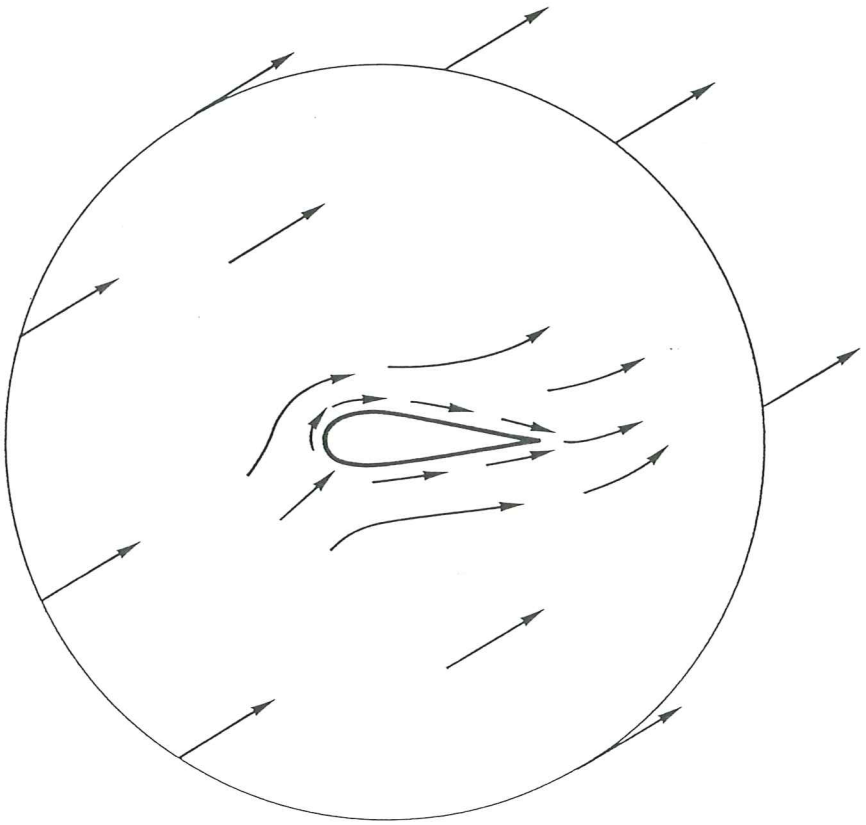

5. RESULTS.

Presented in this section are the various results obtained in testing the previously outlined programs. Due to the nature of the program output, the majority of the results will be demonstrated using "hardcopy" from the FLAVIA post processor program. The results have been collected together and appear as appendices 1 to 4, inclusive. In this section, supplementary description will be given to augment the presented results together with an analytical technique which was used to verify the results obtained.

Appendix 2 gives output from FLAVIA for the test case of a N.A.C.A. 0012 under the following conditions:

$U_\infty = 10.0$, the freestream velocity.

$\alpha = 10.0°$, the aerofoil angle of attack.

The following is a description of the plates that are given in appendix 2.

Plate 1: Shows the full mesh used for the calculation procedure.

Plate 2: Shows the detail of the mesh around the aerofoil.

Plate 3: Shows the complete potential field calculated by the "non-lifting" potential solver.

Plate 4: Shows the stream lines around the aerofoil according to the output from the "non-lifting" potential solver. The rear stagnation point can be clearly seen on the upper surface.

Plate 5: Shows the stream lines around the aerofoil after 9 iterations of the process. This is after the solution was seen to converge and is the final solution. The changes in the front and rear stagnation points (from plate 1) can clearly be seen and indeed, the rear stagnation point is at the trailing edge.

Plate 6: Shows the graph of Cp around the aerofoil (plotted against x direction) together with a representation of the velocity vectors around the aerofoil.

Appendix 3. gives results from a similar test conducted for the same N.A.C.A. 0012 but with the following conditions:

$U_\infty = 10.0$

$\alpha = 45°$

This is an extreme case and it must be remembered that in real viscous flow, the flow would have separated at an angle of attack considerably lower than this. It is presented here, however, to show clearly the stages towards the converged solution.

Plate 1: Shows the streamlines in the "non-lifting" potential field. The rear stagnation point is seen to occur well up the upper surface of the aerofoil.

Plate 2: Shows the streamlines of the applied corrective circulation field.

Plate 3: Shows the streamline pattern after 1 iteration. The solution is seen to have over compensated and has applied too much circulation and the rear stagnation point is seen to occur on the lower surface.

Plate 4: Shows the streamline pattern after 4 iterations. The solver is seen to have compensated for the original overshoot but has overshot the correction but to a much lower degree than in Plate 2. The rear stagnation point is seen on the upper surface.

Plate 5: Shows the streamlines for the converged solution. The flow is seen to smoothly leave the trailing edge.

Appendix 4 gives tabular and graphical information on the convergence of the solutions for the two test cases mentioned above. The tabular data shows the calculated values of the normal velocity at the trailing edge, the calculated value of circulation required to correct it and the running total of the circulation for each iteration step.

Also in appendix 4, the convergence data is shown graphically. The difference between successive values of the normal velocity at the trailing edge (vte) is plotted against the number of iteration cycles for both test cases. Presented also, are graphs of the variation of the total value of circulation versus number of iteration steps for both test cases.

In order to validate the calculated results, it was desired to make a simple analytical estimate of the circulation. To do this Lifting-line (or Thin Aerofoil) theory was used. The fundamental equation of Thin Aerofoil theory is:

$$\frac{1}{2\pi}\int_0^c \frac{\gamma(\xi)d\xi}{x-\xi} = V_\infty\left(\alpha - \frac{dz}{dx}\right) \qquad 5.(1).$$

This is simply a statement that the camber line is a streamline of the flow. For the case of a symmetrical aerofoil, there is no camber and thus the camber line is coincident with the chord line. This reduces 5.(1). to:

$$\frac{1}{2\pi}\int_0^c \frac{\gamma(\xi)d\xi}{x-\xi} = V_\infty\alpha \qquad 5.(2).$$

In essence, Thin Aerofoil theory treats a symmetrical aerofoil as a flat plate and thus this model does not account for the aerofoil thickness distribution. Equation 5.(2). is an *exact* expression for the inviscid, incompressible flow over a flat plate at an angle of attack.

In order to integrate 5.(2)., transform ξ into θ by the following transformation:

$$\xi = \frac{c}{2}(1 - cos\ \theta) \qquad 5.(3).$$

Since x is a fixed point, it corresponds to a particular value of θ, namely θ_0, so that:

$$x = \frac{c}{2}(1 - cos\ \theta_0) \qquad 5.(4).$$

and:

$$d\xi = \frac{c}{2}sin\ \theta d\theta \qquad 5.(5).$$

Now, substituting 5.(3). and 5.(5). into 5.(2). an expression for the vorticity can be obtained (noting the change in the limits of integration):

$$\gamma(\theta) = 2\alpha V_\infty \frac{(1 + cos\ \theta)}{sin\ \theta} \qquad 5.(6).$$

Now apply the Kutta condition such that the vorticity at the trailing edge is 0. Then applying L'Hopital's rule on 5.(6). gives:

$$\gamma(\pi) = 2\alpha V_\infty \frac{-sin\ \pi}{cos\ \pi} = 0 \qquad 5.(7).$$

The circulation is now the integral of the vorticity:

$$\Gamma = \int_0^c \gamma(\xi) d\xi \qquad 5.(8).$$

Giving, for a symmetrical aerofoil:

$$\Gamma = \pi.\alpha.\mathbf{c}.\mathbf{V}_\infty \qquad 5.(9).$$

Appendix 4. also gives these theoretical values of circulation for the tested aerofoils.

6. DISCUSSION.

Examination of the results given in appendix 4. shows that the method is relatively quick to converge to the final value of circulation (in ~7 cycles for the extreme case). This behaviour has been seen to occur throughout a full range of incidences ($0° \leq \alpha \leq 45°$), so the solution is seen to be reasonably stable.

It can be seen from analysis of the results presented in appendix 4., however, that there is a tendency to "overshoot" the desired result and then it is seen to oscillate around the final solution with diminishing amplitude for successive iterations until convergence.

Inspection of the FLAVIA graphical output shows the expected streamline patterns and the sequence of appendix 3. clearly shows the "overshoot" and subsequent oscillations in trailing edge position as the solution converges.

Also presented in appendices 2. and 3. are graphs of pressure coefficient (plotted around the aerofoil) together with the velocity vectors, for the two primary test cases. The general form of the Cp curves is good and indeed, the values correspond quite well with the published data in reference 1. However, closer examination of the results shows certain aberrations in the velocity vectors (and consequently in the Cp values) around the surface of the aerofoil.

As stated earlier in this report, the calculated nodal velocities are further approximations of the already approximate elemental values. Thus, although the normal velocities, calculated on the aerofoil surface due to the circulation (theoretically the only component) are exact, the imposition of the negative of these velocities as applied "loads" in the potential solver does not exactly yield the desired normal nodal velocity in the opposite direction to remove these "loads". Thus, on each iteration, a slight error is incurred, and as the iteration process is continued these errors are summed and may well accumulate into appreciable error by the end of the iteration process.

This error can be diminished by using many small elements near the aerofoil surface, but this would have obvious penalties in terms of computation time and thus expense. Alternatively, the iteration process itself may be adjusted to try to minimise the error. Instead of continually summing the successive velocity fields, save the initial "non-lifting" velocity field, then run (say) two cycles of the iteration process and note the culminated circulation. Then calculate the velocity field due to this circulation and add it to the original "non-lifting" field, then re-start the iteration process for another two cycles and again note the circulation and keep repeating the process always summing the most current circulation field with the original "non-lifting" field. In this way it is hoped that the culmination of error may be minimised.

Comparison of the numerical results with those predicted by the Lifting-line theory shows that for the extreme case of $\alpha = 45°$, the agreement is excellent (~0.04% error). However, for the moderate case of $\alpha = 10°$, the agreement is less good, with the numerical solution overestimating the circulation by approximately 9%. It must be remembered that the Lifting-line theory takes no account of the thickness of the aerofoil and at the lower angle of attack the effect of thickness would be greater. However, the Lifting-line theory is known to give very good results for slender aerofoils (the N.A.C.A. 0012 aerofoil is considered to be the "fattest" slender aerofoil) and thus this cannot be the sole reason for the discrepancy. The other main possible source of error occurs in the numerical solution itself as, around the trailing edge there is a high gradient in velocities (the sharper the trailing edge, the greater the gradient) and this will tend to push the limitations of the Finite Element approximation, possibly leading to erroneous values in the calculated elemental velocities around the trailing edge. This is not, however, a consistent reason since, for the higher angle of attack case (where the velocity gradients at the trailing edge are greater) better results are obtained. In the absence of a satisfactory explanation of this effect, it has to remain a topic for further investigation.

It must be noted that the potential theory described here gives the erroneous prediction of zero drag. In real flow, viscous effects cause skin friction and separation which inevitably produce finite drag. The inviscid flow described here simply does not model the proper physics for drag calculations. On the other hand, it is seen that the prediction of lift is quite realistic.

Inevitably, for any numerical solution technique which attempts to solve general potential flow problems, comparisons must be drawn with the classic panel methods. Traditional panel methods approximate a body to a series of straight "panels" each carrying a given source or sink strength per unit length.

The values of these sources are calculated with regard to the freestream conditions, so that the desired body shape becomes a streamline of the flow. In this way, the "non-lifting" potential field due to the body can be calculated. From the source panel values, the velocities tangential to each panel may be calculated and hence the pressure coefficient may be obtained directly from a modified form of Bernoulli's equation, namely:

$$C_p = 1 - \left(\frac{V}{V_\infty}\right)^2 \qquad 6.(1).$$

The above source panel method, only gives non-lifting solutions (sources and sinks have no circulation); as has been seen, it is usually desired to calculate the lifting solution. To do this, the above method may be augmented by using the Vortex Panel method in which the body shape is

modelled by series of constant strength vortex panels distributed over the surface of the aerofoil.

The idea of the Vortex Panel method is similar to the idea of the Lifting-line theory in which the vortex sheet is spread along the camber line (rather than over the complete surface). The equations which are used to solve the Vortex Panel method are similar in many respects to those which are used to solve the Source Panel methods. At the trailing edge, however, the similarity ends as for the Vortex Panel method the Kutta condition must be applied. This can be done in a number of ways, for example, the vortex strength in the upper and lower trailing edge panels can be set to an equal and opposite value thus, the value of vorticity will be zero at the trailing edge where the two panels meet (which is another way of expressing the Kutta condition).

The Vortex Panel method does offer some advantages over the method formulated in this report. For example, in the Vortex Panel method it is not necessary to approximate the position of a point vortex, responsible for all circulation, to the 1/4 chord point, this is particularly important for non-wing applications such as automobile or submarine aerodynamics. Also, the tangential velocities panel velocities calculated by this method have been shown to be very accurate which in turn leads to a very accurate pressure coefficient distribution where as in the Finite Element method, the tangential velocities that are calculated on the aerofoil surface are greater approximations and thus less accurate.

However, the Vortex Panel method described in this section is termed a "first-order" method as it assumes a constant value of vorticity over a given panel. Although the method may appear to be straightforward, a review of the available literature shows that it can prove frustrating in the numerical implementation. For example, the results for a given body are sensitive to the number of panels used, their various sizes and the way they are distributed over the body surface (ie. it is usually advantageous to place a large number of small panels near the leading and trailing edges of an aerofoil and a smaller number of larger panels in the middle). There is also a need to ignore one control point (point in the middle of a panel) in order to have a determined system in n equations of n unknowns and this introduces further arbitrariness into the numerical solution as different choices of removed control points can yield differences in the solution. Moreover, the resulting numerical vorticity distribution is not always smooth, but rather they have oscillations from one panel to the next as a result of numerical inaccuracies. The problems mentioned above are generally overcome in different ways by different groups who have developed relatively sophisticated panel programs for practical use.

Such accuracy problems have encouraged the development of higher order panel methods. These higher order methods are now in industrial use and provide excellent low Mach, low angle of attack predictions. However, the associated complexities involved with the higher order

methods are of a similar "scale" as the increase in complexities required to improve the Finite Element solution and thus, even though the Finite Element method does not predict the pressure distribution to the same degree of accuracy as panel methods, the implementation of such a procedure is much simpler and often it is only an accurate prediction of lift which is required and as has been seen, this can be obtained directly from an accurate prediction of the circulation via the Kutta-Joukowski theorem. Moreover, the Vortex Panel method is a very specific solution for potential flow whereas the general Finite Element techniques developed here can be easily expanded to more complex descriptive equations such as the Full Potential, Euler or time averaged Navier-Stokes equations.

It may be concluded then, that the approach described in this report represents a relatively easy to implement procedure that offers good lift results but only moderate pressure distribution results. Moreover, the general approach lends itself easily to the solution of more complex physical equations.

In order to take advantage of the possible benefits of this solution scheme it is desired that the solution should be as quick to resolve as possible, to this end, the chosen equation solver had to be re-evaluated.

Already existent in the original two dimensional quasi-harmonic equation program was a "frontal" solver routine which was used throughout the development of the codes. Frontal solvers offer the advantage that they do not require large amounts of on board memory, however, frontal solvers are slow as they require large amounts of information exchange with the disc. On the Convex "supercomputer", these limitations of on board memory do not apply and thus, an alternative, faster, solution scheme may be sought.

The chosen alternative was to use the Conjugate Gradient Algorithm, which is a solution scheme which aims to minimise the residual (or error) derived in a given system of equations. The algorithm for the method is given below:

For a system:

$$A.x = b$$

Where A is a matrix and x and b are vectors. Then define a residual, r, such that:

$$r^k = b - A.x^k$$

Where k is the step number and x is some starting value of the vector x. Then select a search

direction, p, such that:

$$p^k = r^k \qquad \text{for } k = 1$$

$$r^k + \alpha_k . p^{k-1} \qquad \text{for } k > 1$$

Where α_k is a coefficient given by:

$$\alpha_K = -\frac{r^{K^T} A p^{K-1}}{p^{K-1^T} A p^{K-1}}$$

Then a coefficient that assesses the amount that the solution moves in the calculated search direction is calculated:

$$\lambda_K = \frac{p^{K^T} r^K}{p^{K^T} A p^K}$$

Then a new value of x may be calculated:

$$x^{k+1} = x^k + \lambda_k . p^k$$

The residual is then re-calculated for k = k+1 and the cycle is continued until convergence.

It is noted that the first cycle of the process is the same as for the Gradient of Steepest Descent method.

The Conjugate Gradient method is one of the fastest to converge. Indeed, in a recent test conducted by Messes A. Hanganu and I. Colominas (both of C.I.M.N.E.), in the solution of 169x169 system of equations, the Conjugate Gradient Algorithm was found to be 10 times faster than the Gradient of Steepest Descent method and 5 times faster than the Gauss-Seidel method. Thus, it is seen that considerable benefits may be seen with the use of the Conjugate Gradient Algorithm to solve the equation system created by the Finite Element Method for this problem.

Further improvements to the solution process may be obtained by applying adaptive meshing techniques with the "non-lifting" potential solver. These techniques are based around the definition of some residual or error term. In this case it would be possible to calculate an error between the discontinuous elemental velocity field and a "smoothed" velocity field (smoothed, for example, by the elemental shape functions). The mesh could then be optimised to minimise this error to some global value (see reference 5.).

There are two drawbacks of this technique, firstly, a general constraint is that the governing equations have to be elliptic (Laplace or Euler, for example) and secondly, the calculation of the error term requires the integration of a product of velocities which requires the use of (at least) six noded triangular elements requiring reprograming to calculate the residual. A further drawback is that, for the circulation field, it is not possible to calculate an error term, since the field is an analytical field and thus, continuous. Hence, the optimisation can only be applied to the initial "non-lifting" solution and this will consequently limit the benefits obtained. Undoubtedly, however, this technique would improve the efficiency of the overall methodology.

7. CONCLUSIONS.

The solution technique, described in this report, delivers acceptable predictions of the circulation (and thus lift) around a two dimensional aerofoil in inviscid irrotational flow. Indeed, these results offer acceptable description of the lift experienced by an aerofoil in low speed, moderate angle of attack flow.

The model also gave the prediction of zero drag which is known to be erroneous. This occurs because the model contains no viscosity and it is viscosity, through the action of skin friction and forcing separation, which is ultimately responsible for creating drag.

The generated results were validated against both experimental data and theoretical predictions from the Lifting-line theory.

Further, the applied technique was found to be a simpler to implement alternative to the established Vortex Panel methods. However, there is an associated cost in overall accuracy, particularly in the predictions of the pressure distribution around the aerofoil.

The general Finite Element Method presented here has the advantage that it offers much wider applicability to the solution of equations which offer broader validity in the physical domain.

REFERENCES.

1. "FUNDAMENTALS OF AERODYNAMICS"
   John D. Anderson Jr.
   Mc.Graw Hill.

2. "PRINCIPLES OF IDEAL FLOW AERODYNAMICS"
   K. Karamcheti.
   John Wiley & Sons.

3. "FOUNDATIONS OF AERODYNAMICS: Bases Of Aerodynamic Design"
   Arnold M.Kuethe & Chuen-Yen Chow.
   John Wiley & Sons.

4. "AN INTRODUCTION TO FINITE ELEMENT COMPUTATIONS"
   E. Hinton & D.R.J. Owen.
   Pineridge Press.

5. "MESH GENERATION IN C.F.D."
   N. P. Weatherill.
   von Karmen Institute For Fluid Dynamics Lecture Series 1989-04.

ACKNOWLEDGMENTS.

The author would like to thank the following for their kind help and support throughout the duration of the project.

Professors E. Oñate, J. M. Canet and Dr. J. Peraire for their help in the development of the applied methodology and their continued support through the program development.

Drs G. Bugeda, F. Quintana and Mr. R. Kreiner for their help with auxiliary data and programs which greatly smoothed the path of the author.

The author has also greatly benefitted from numerous discussions with his colleagues Dr. R. Codina, Mr. F. Escalante, Mr. J. Castro, Mr. F. Bassas, Mr. A. Hanganu and Mr. I. Colominas.

Thanks must also go to the secretaries of the C.I.M.N.E. who have been more than obliging throughout the author's time in Barcelona. Finally, special thanks goes to Ms. Edith Wolf, without who's help this report would not have been presented in time.

Appendix 1.

Flowchart Of Process.

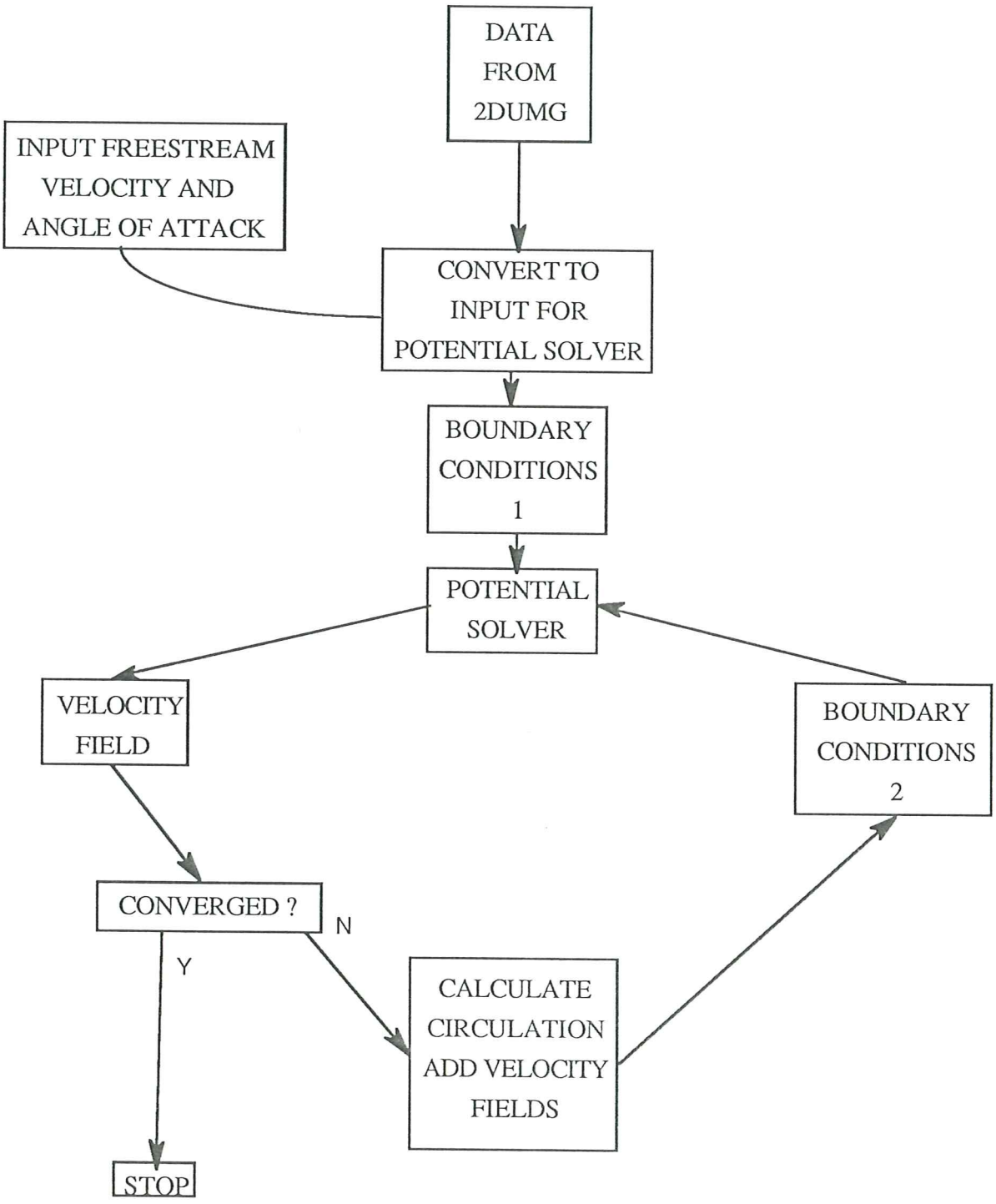
DATA FROM 2DUMG
INPUT FREESTREAM VELOCITY AND ANGLE OF ATTACK
CONVERT TO INPUT FOR POTENTIAL SOLVER
BOUNDARY CONDITIONS 1
POTENTIAL SOLVER
VELOCITY FIELD
BOUNDARY CONDITIONS 2
CONVERGED ?
N
Y
CALCULATE CIRCULATION ADD VELOCITY FIELDS
STOP

Appendix 2.

FLAVIA Results For Test Case With

$\alpha = 10°$

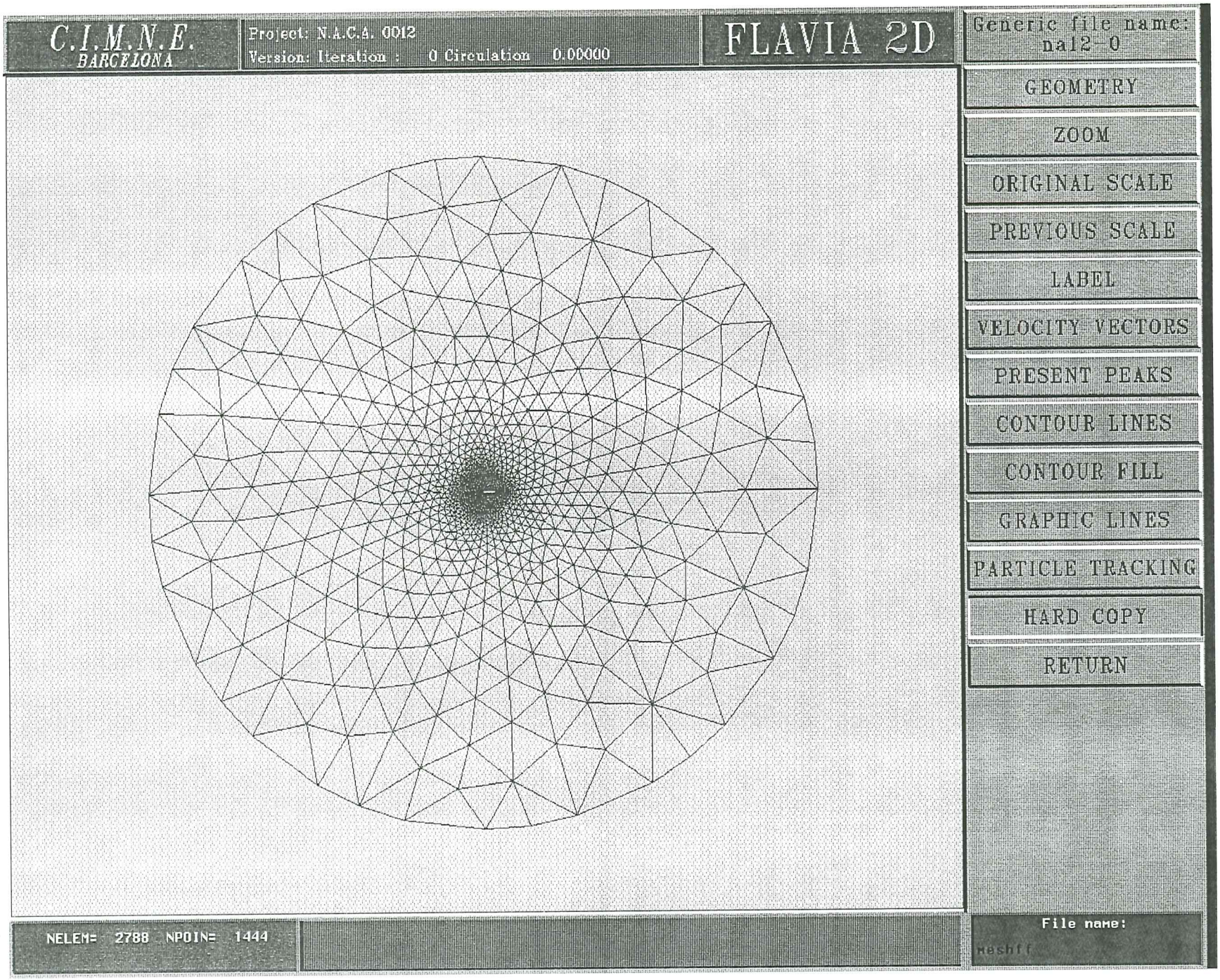
C.I.M.N.E.
BARCELONA
Project: N.A.C.A. 0012
Version: Iteration : 0 Circulation 0.00000
FLAVIA 2D
Generic file name:
na12-0
GEOMETRY
ZOOM
ORIGINAL SCALE
PREVIOUS SCALE
LABEL
VELOCITY VECTORS
PRESENT PEAKS
CONTOUR LINES
CONTOUR FILL
GRAPHIC LINES
PARTICLE TRACKING
HARD COPY
RETURN
NELEM= 2788 NPOIN= 1444
File name:
meshff

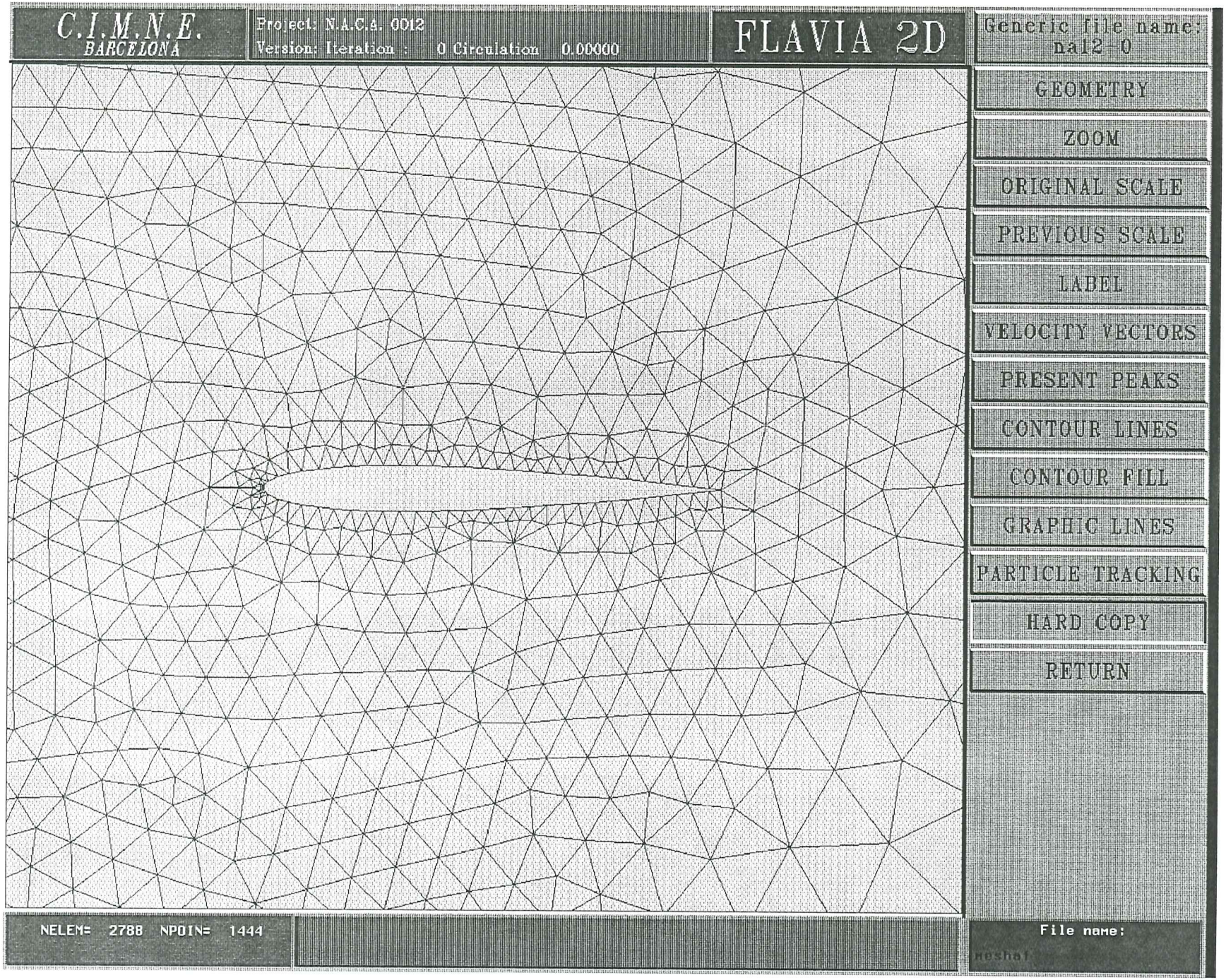
C.I.M.N.E.
BARCELONA
Project: N.A.C.A. 0012
Version: Iteration : 0 Circulation 0.00000
FLAVIA 2D
Generic file name:
na12 0
GEOMETRY
ZOOM
ORIGINAL SCALE
PREVIOUS SCALE
LABEL
VELOCITY VECTORS
PRESENT PEAKS
CONTOUR LINES
CONTOUR FILL
GRAPHIC LINES
PARTICLE TRACKING
HARD COPY
RETURN
NELEM= 2788 NPOIN= 1444
File name:
meshaf

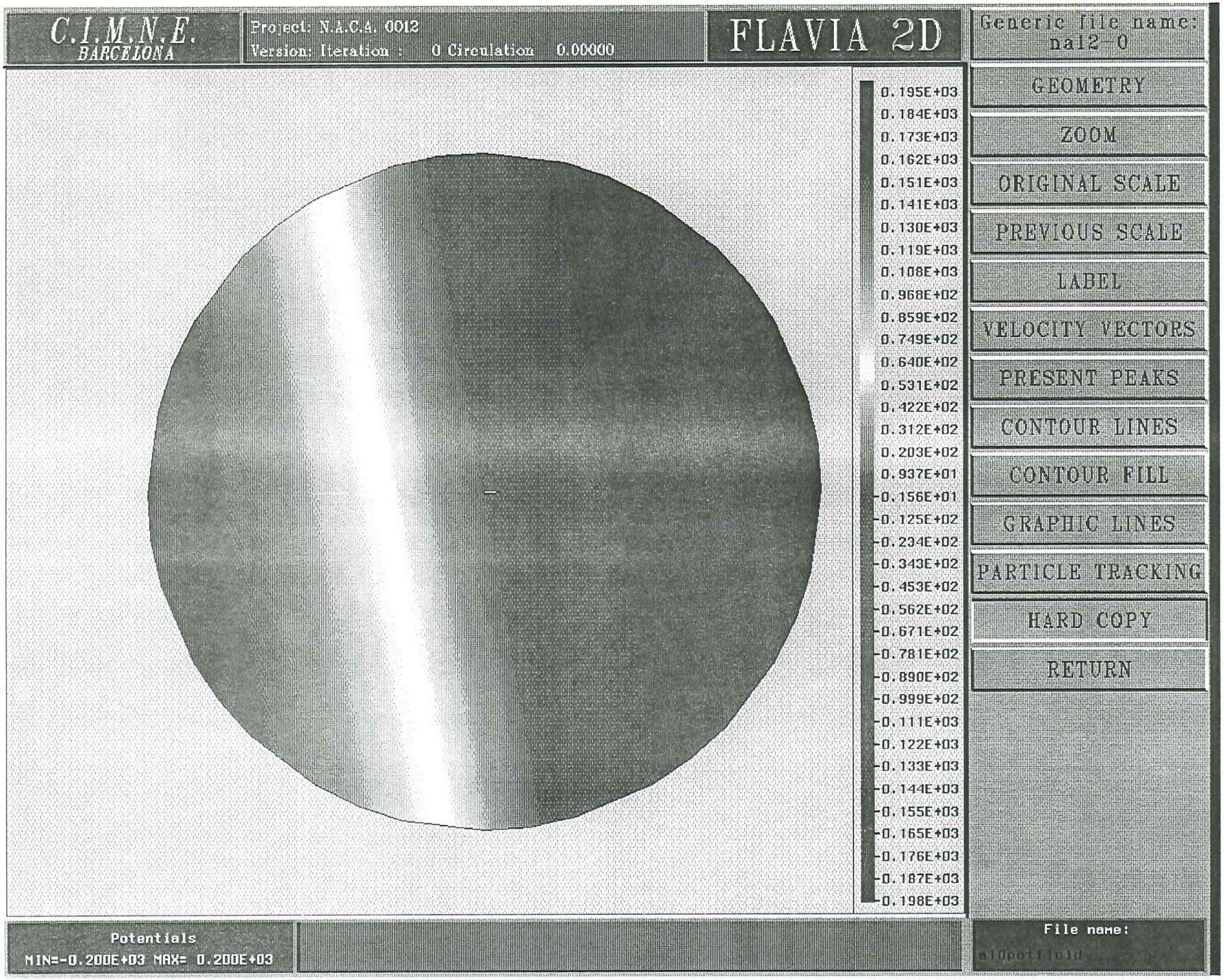
C.I.M.N.E.
BARCELONA
Project: N.A.C.A. 0012
Version: Iteration : 0 Circulation 0.00000
FLAVIA 2D
Generic file name:
na12-0
0.195E+03
0.184E+03
0.173E+03
0.162E+03
0.151E+03
0.141E+03
0.130E+03
0.119E+03
0.108E+03
0.968E+02
0.859E+02
0.749E+02
0.640E+02
0.531E+02
0.422E+02
0.312E+02
0.203E+02
0.937E+01
-0.156E+01
-0.125E+02
-0.234E+02
-0.343E+02
-0.453E+02
-0.562E+02
-0.671E+02
-0.781E+02
-0.890E+02
-0.999E+02
-0.111E+03
-0.122E+03
-0.133E+03
-0.144E+03
-0.155E+03
-0.165E+03
-0.176E+03
-0.187E+03
-0.198E+03
GEOMETRY
ZOOM
ORIGINAL SCALE
PREVIOUS SCALE
LABEL
VELOCITY VECTORS
PRESENT PEAKS
CONTOUR LINES
CONTOUR FILL
GRAPHIC LINES
PARTICLE TRACKING
HARD COPY
RETURN
Potentials
MIN=-0.200E+03 MAX= 0.200E+03
File name:
a10potfield

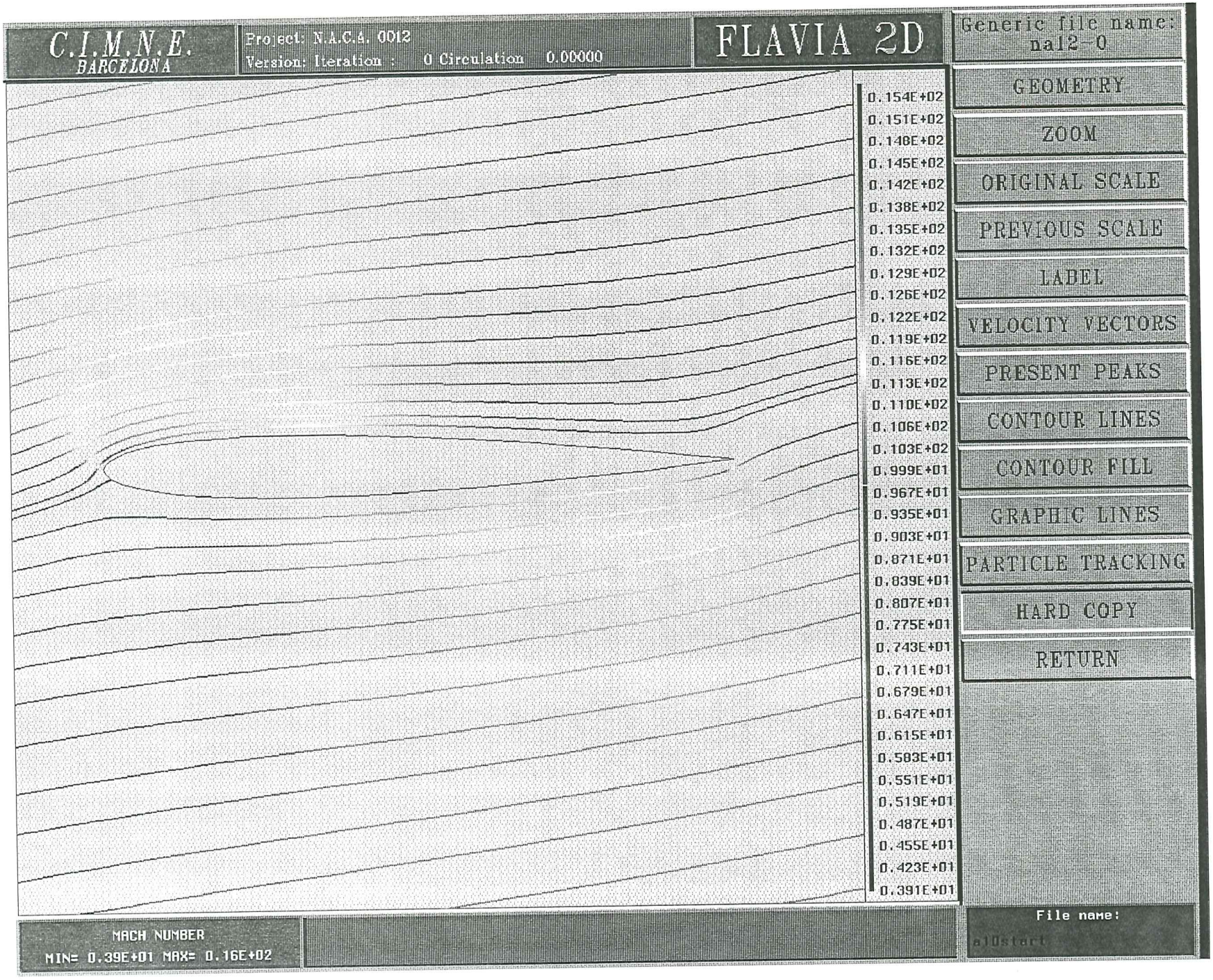
C.I.M.N.E.
BARCELONA
Project: N.A.C.A. 0012
Version: Iteration : 0 Circulation 0.00000
FLAVIA 2D
Generic file name:
na12-0
GEOMETRY
ZOOM
ORIGINAL SCALE
PREVIOUS SCALE
LABEL
VELOCITY VECTORS
PRESENT PEAKS
CONTOUR LINES
CONTOUR FILL
GRAPHIC LINES
PARTICLE TRACKING
HARD COPY
RETURN
0.154E+02
0.151E+02
0.148E+02
0.145E+02
0.142E+02
0.138E+02
0.135E+02
0.132E+02
0.129E+02
0.126E+02
0.122E+02
0.119E+02
0.116E+02
0.113E+02
0.110E+02
0.106E+02
0.103E+02
0.999E+01
0.967E+01
0.935E+01
0.903E+01
0.871E+01
0.839E+01
0.807E+01
0.775E+01
0.743E+01
0.711E+01
0.679E+01
0.647E+01
0.615E+01
0.583E+01
0.551E+01
0.519E+01
0.487E+01
0.455E+01
0.423E+01
0.391E+01
MACH NUMBER
MIN= 0.39E+01 MAX= 0.16E+02
File name:
a10start

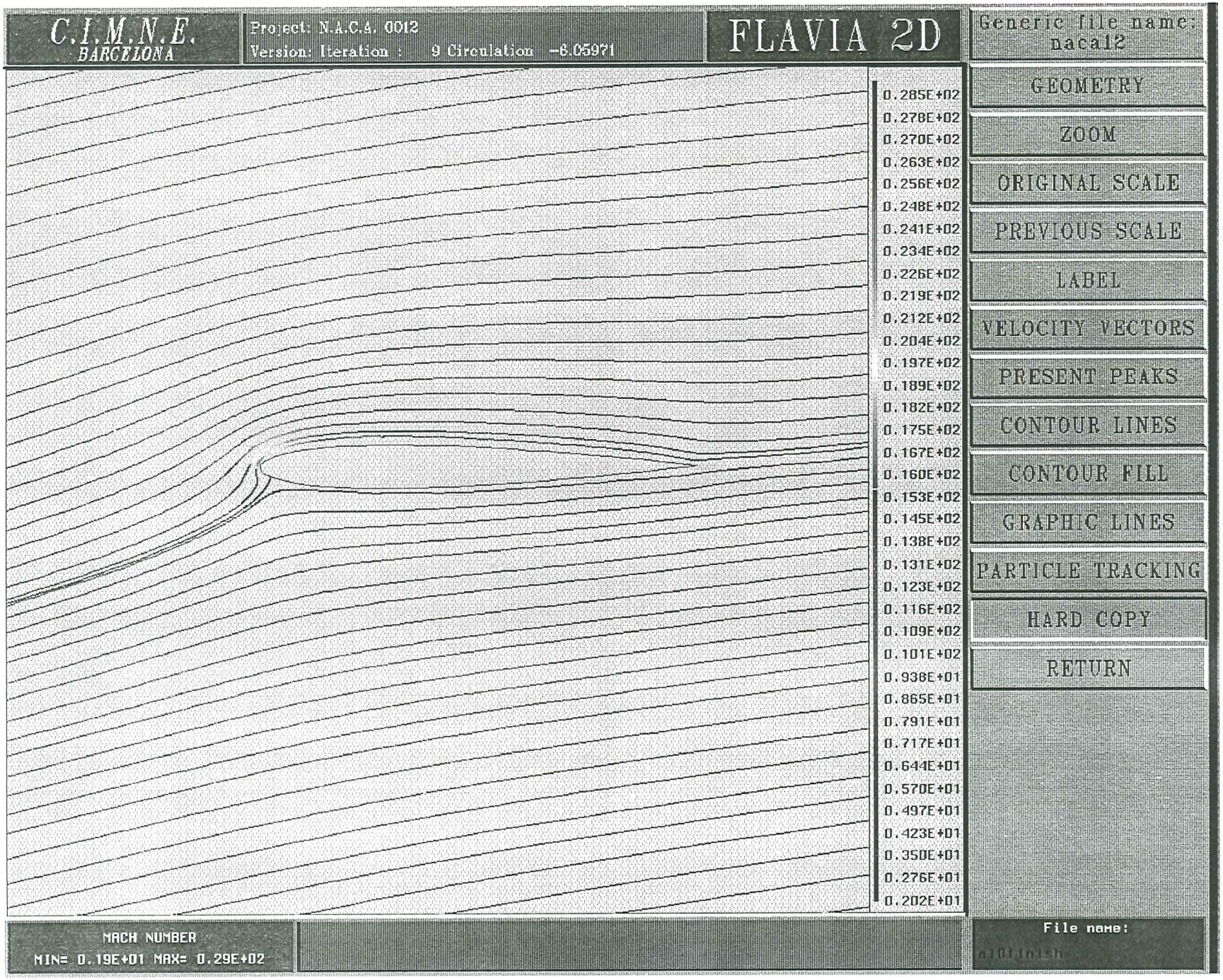
C.I.M.N.E.
BARCELONA
Project: N.A.C.A. 0012
Version: Iteration : 9 Circulation -6.05971
FLAVIA 2D
Generic file name: naca12
GEOMETRY
ZOOM
ORIGINAL SCALE
PREVIOUS SCALE
LABEL
VELOCITY VECTORS
PRESENT PEAKS
CONTOUR LINES
CONTOUR FILL
GRAPHIC LINES
PARTICLE TRACKING
HARD COPY
RETURN
0.285E+02
0.278E+02
0.270E+02
0.263E+02
0.256E+02
0.248E+02
0.241E+02
0.234E+02
0.226E+02
0.219E+02
0.212E+02
0.204E+02
0.197E+02
0.189E+02
0.182E+02
0.175E+02
0.167E+02
0.160E+02
0.153E+02
0.145E+02
0.138E+02
0.131E+02
0.123E+02
0.116E+02
0.109E+02
0.101E+02
0.938E+01
0.865E+01
0.791E+01
0.717E+01
0.644E+01
0.570E+01
0.497E+01
0.423E+01
0.350E+01
0.276E+01
0.202E+01
MACH NUMBER
MIN= 0.19E+01 MAX= 0.29E+02
File name:

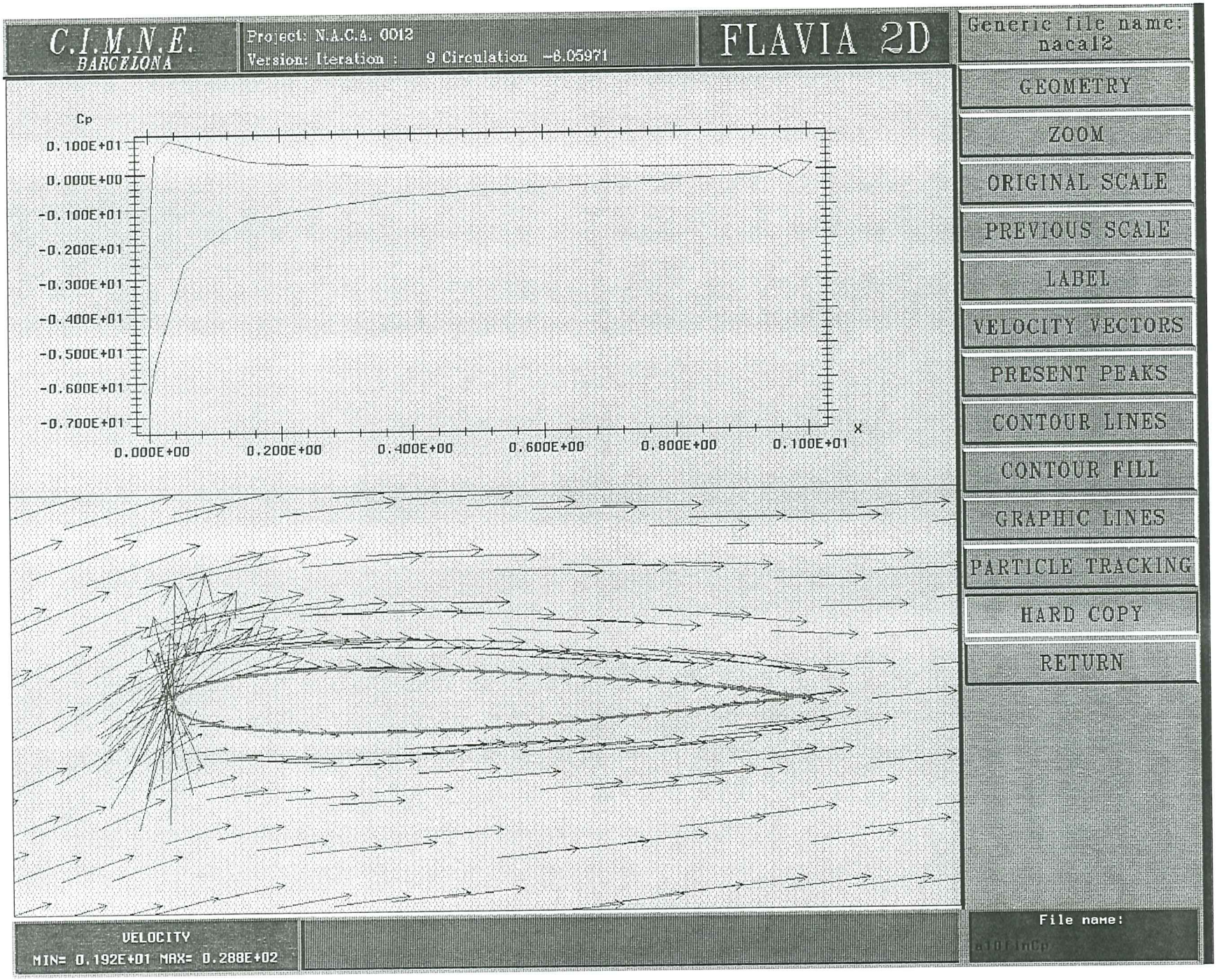
C.I.M.N.E.
BARCELONA
Project: N.A.C.A. 0012
Version: Iteration : 9 Circulation -8.05971
FLAVIA 2D
Generic file name: naca12
GEOMETRY
ZOOM
ORIGINAL SCALE
PREVIOUS SCALE
LABEL
VELOCITY VECTORS
PRESENT PEAKS
CONTOUR LINES
CONTOUR FILL
GRAPHIC LINES
PARTICLE TRACKING
HARD COPY
RETURN
Cp
0.100E+01
0.000E+00
-0.100E+01
-0.200E+01
-0.300E+01
-0.400E+01
-0.500E+01
-0.600E+01
-0.700E+01
X
0.000E+00
0.200E+00
0.400E+00
0.600E+00
0.800E+00
0.100E+01
VELOCITY
MIN= 0.192E+01 MAX= 0.288E+02
File name:

Appendix 3.

FLAVIA Results For Test Case With

$\alpha = 45°$

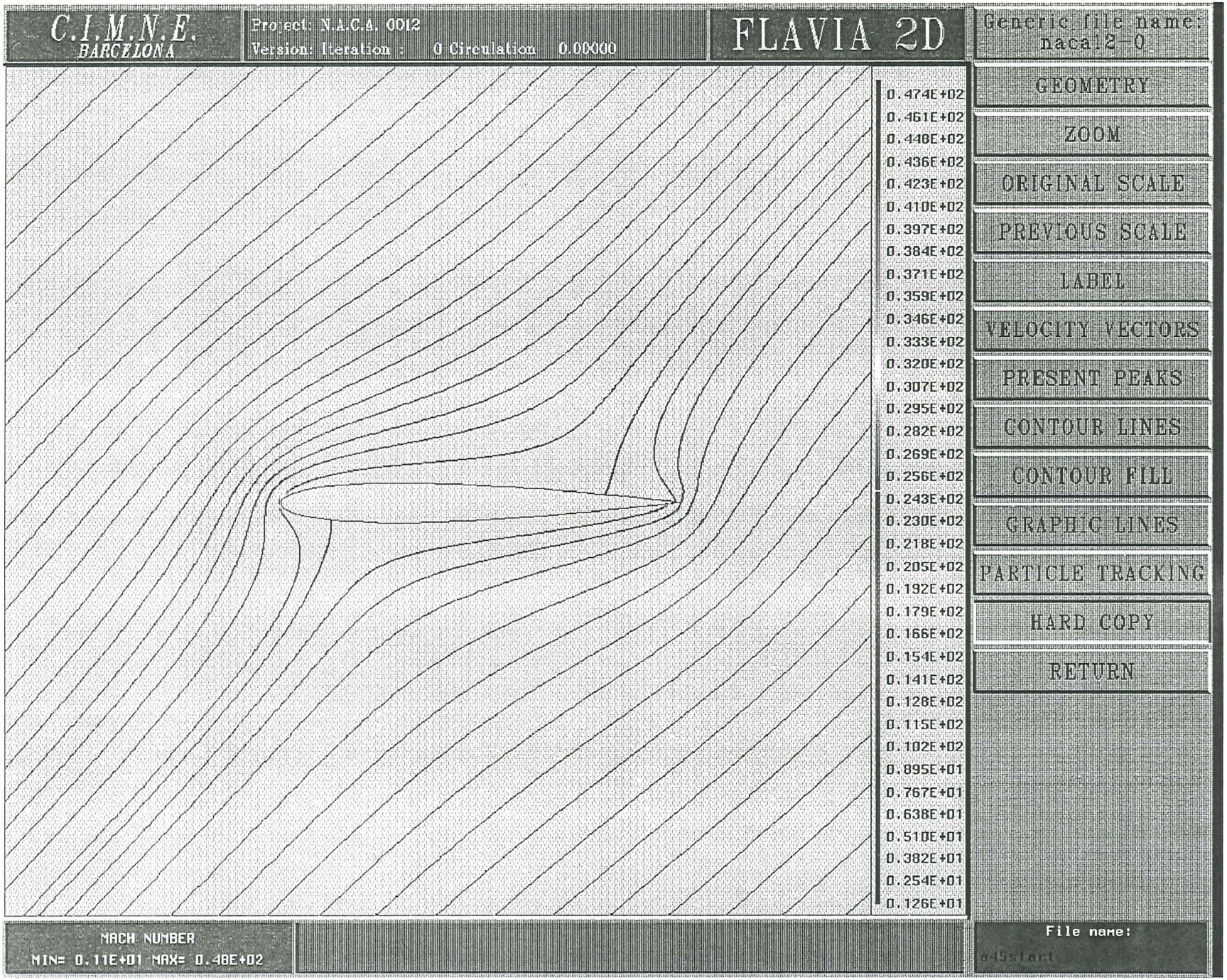
C.I.M.N.E.
BARCELONA
Project: N.A.C.A. 0012
Version: Iteration : 0 Circulation 0.00000
FLAVIA 2D
Generic file name:
naca12 0
GEOMETRY
ZOOM
ORIGINAL SCALE
PREVIOUS SCALE
LABEL
VELOCITY VECTORS
PRESENT PEAKS
CONTOUR LINES
CONTOUR FILL
GRAPHIC LINES
PARTICLE TRACKING
HARD COPY
RETURN
0.474E+02
0.461E+02
0.448E+02
0.436E+02
0.423E+02
0.410E+02
0.397E+02
0.384E+02
0.371E+02
0.359E+02
0.346E+02
0.333E+02
0.320E+02
0.307E+02
0.295E+02
0.282E+02
0.269E+02
0.256E+02
0.243E+02
0.230E+02
0.218E+02
0.205E+02
0.192E+02
0.179E+02
0.166E+02
0.154E+02
0.141E+02
0.128E+02
0.115E+02
0.102E+02
0.895E+01
0.767E+01
0.638E+01
0.510E+01
0.382E+01
0.254E+01
0.126E+01
MACH NUMBER
MIN= 0.11E+01 MAX= 0.48E+02
File name:
a45start

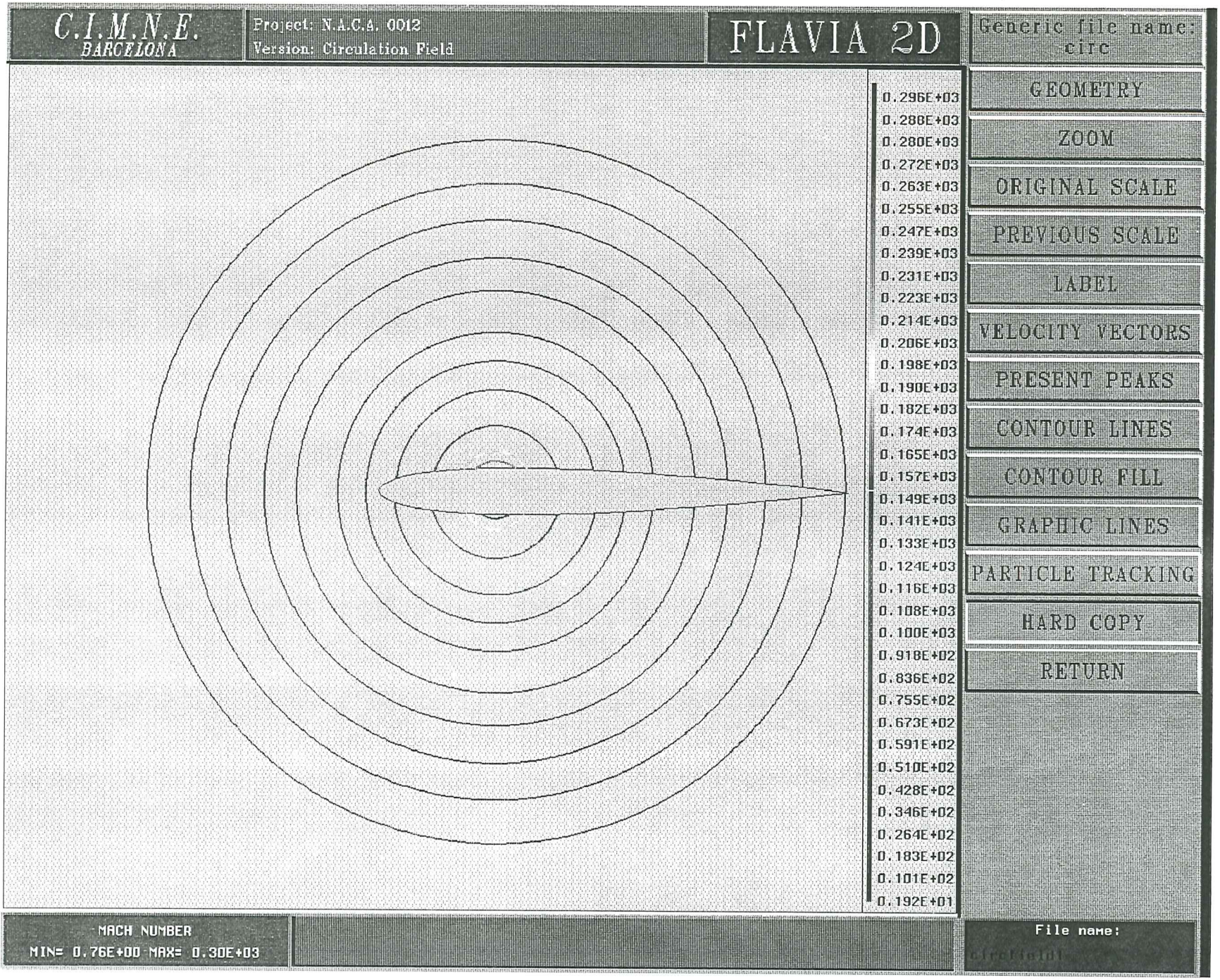
C.I.M.N.E.
BARCELONA
Project: N.A.C.A. 0012
Version: Circulation Field
FLAVIA 2D
Generic file name: circ
GEOMETRY
ZOOM
ORIGINAL SCALE
PREVIOUS SCALE
LABEL
VELOCITY VECTORS
PRESENT PEAKS
CONTOUR LINES
CONTOUR FILL
GRAPHIC LINES
PARTICLE TRACKING
HARD COPY
RETURN
0.296E+03
0.288E+03
0.280E+03
0.272E+03
0.263E+03
0.255E+03
0.247E+03
0.239E+03
0.231E+03
0.223E+03
0.214E+03
0.206E+03
0.198E+03
0.190E+03
0.182E+03
0.174E+03
0.165E+03
0.157E+03
0.149E+03
0.141E+03
0.133E+03
0.124E+03
0.116E+03
0.108E+03
0.100E+03
0.918E+02
0.836E+02
0.755E+02
0.673E+02
0.591E+02
0.510E+02
0.428E+02
0.346E+02
0.264E+02
0.183E+02
0.101E+02
0.192E+01
MACH NUMBER
MIN= 0.76E+00 MAX= 0.30E+03
File name:
circfield

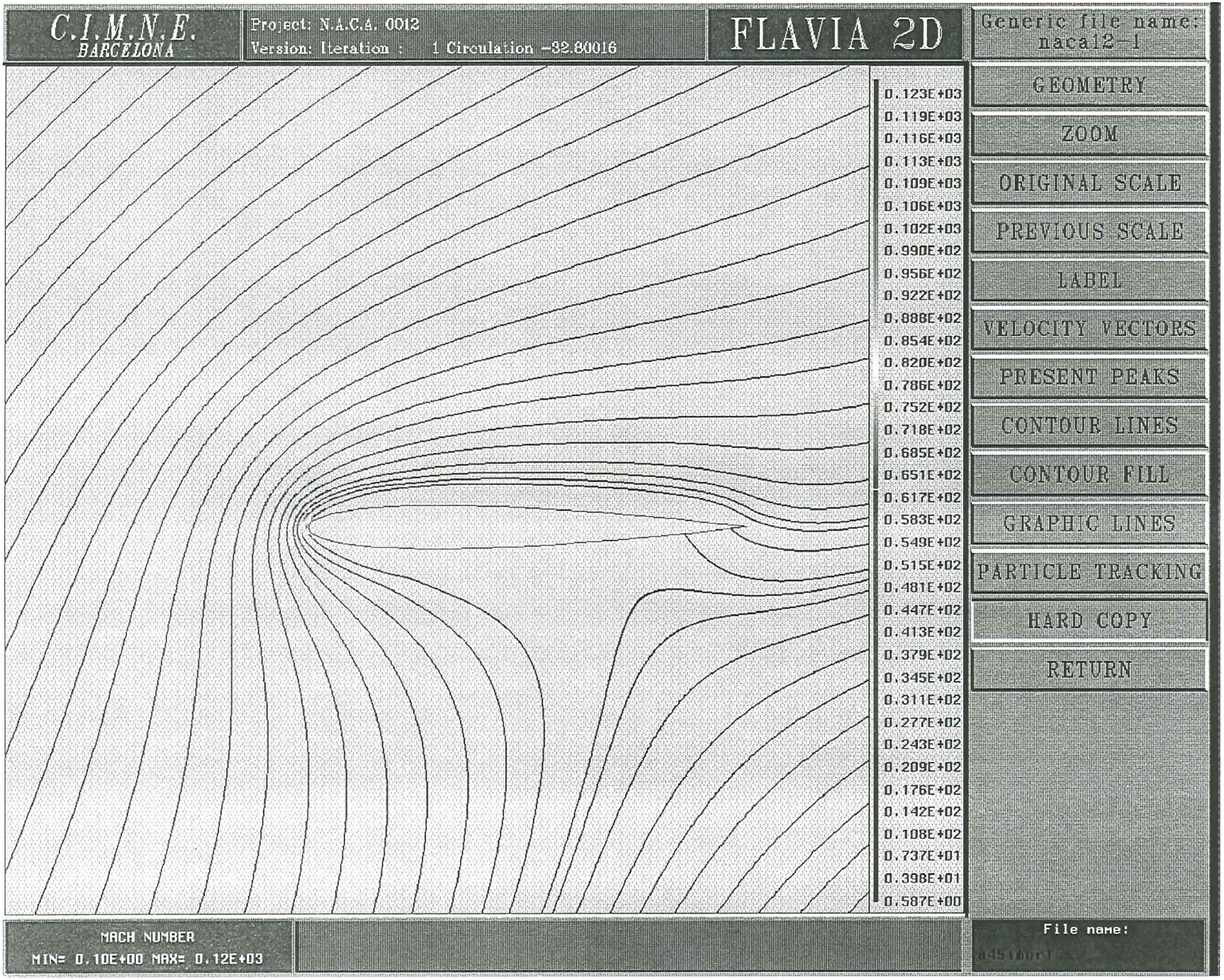
C.I.M.N.E.
BARCELONA
Project: N.A.C.A. 0012
Version: Iteration : 1 Circulation -32.60016
FLAVIA 2D
Generic file name:
naca12-1
GEOMETRY
ZOOM
ORIGINAL SCALE
PREVIOUS SCALE
LABEL
VELOCITY VECTORS
PRESENT PEAKS
CONTOUR LINES
CONTOUR FILL
GRAPHIC LINES
PARTICLE TRACKING
HARD COPY
RETURN
0.123E+03
0.119E+03
0.116E+03
0.113E+03
0.109E+03
0.106E+03
0.102E+03
0.990E+02
0.956E+02
0.922E+02
0.888E+02
0.854E+02
0.820E+02
0.786E+02
0.752E+02
0.718E+02
0.685E+02
0.651E+02
0.617E+02
0.583E+02
0.549E+02
0.515E+02
0.481E+02
0.447E+02
0.413E+02
0.379E+02
0.345E+02
0.311E+02
0.277E+02
0.243E+02
0.209E+02
0.176E+02
0.142E+02
0.108E+02
0.737E+01
0.398E+01
0.587E+00
MACH NUMBER
MIN= 0.10E+00 MAX= 0.12E+03
File name:

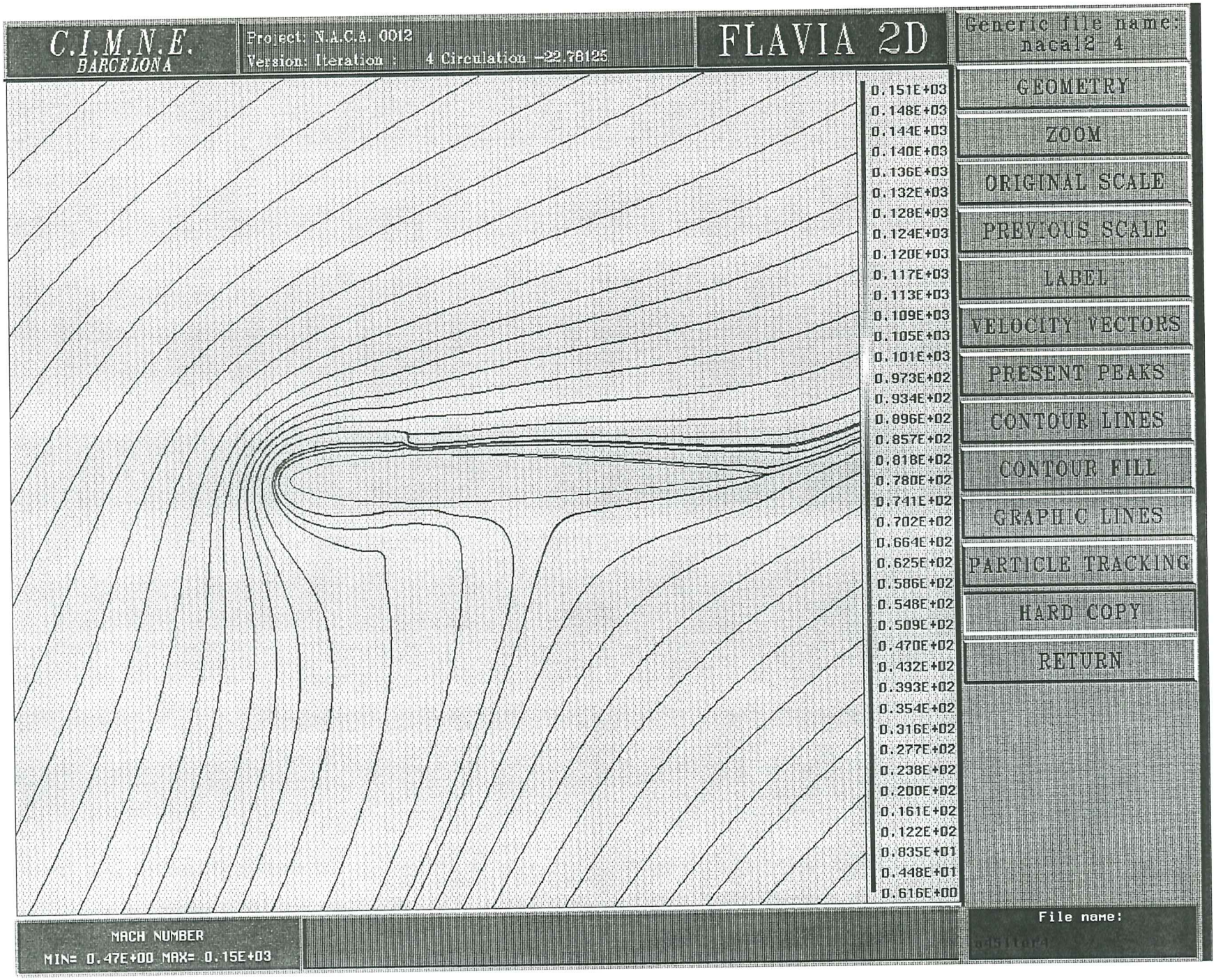
C.I.M.N.E.
BARCELONA
Project: N.A.C.A. 0012
Version: Iteration : 4 Circulation -22.78125
FLAVIA 2D
Generic file name:
naca12-4
0.151E+03
0.148E+03
0.144E+03
0.140E+03
0.136E+03
0.132E+03
0.128E+03
0.124E+03
0.120E+03
0.117E+03
0.113E+03
0.109E+03
0.105E+03
0.101E+03
0.973E+02
0.934E+02
0.896E+02
0.857E+02
0.818E+02
0.780E+02
0.741E+02
0.702E+02
0.664E+02
0.625E+02
0.586E+02
0.548E+02
0.509E+02
0.470E+02
0.432E+02
0.393E+02
0.354E+02
0.316E+02
0.277E+02
0.238E+02
0.200E+02
0.161E+02
0.122E+02
0.835E+01
0.448E+01
0.616E+00
GEOMETRY
ZOOM
ORIGINAL SCALE
PREVIOUS SCALE
LABEL
VELOCITY VECTORS
PRESENT PEAKS
CONTOUR LINES
CONTOUR FILL
GRAPHIC LINES
PARTICLE TRACKING
HARD COPY
RETURN
MACH NUMBER
MIN= 0.47E+00 MAX= 0.15E+03
File name:

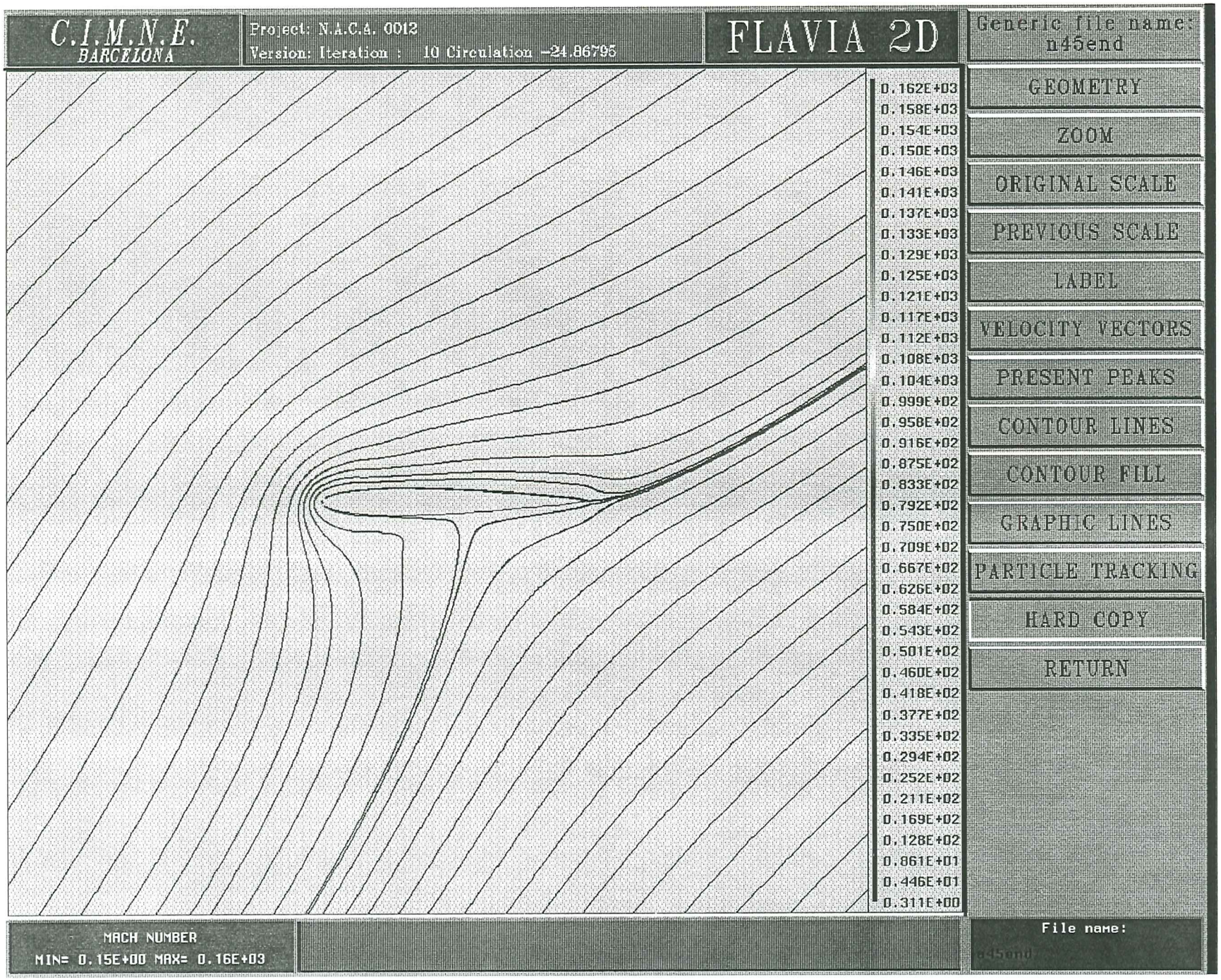
C.I.M.N.E.
BARCELONA
Project: N.A.C.A. 0012
Version: Iteration : 10 Circulation -24.86795
FLAVIA 2D
Generic file name:
n45end
GEOMETRY
ZOOM
ORIGINAL SCALE
PREVIOUS SCALE
LABEL
VELOCITY VECTORS
PRESENT PEAKS
CONTOUR LINES
CONTOUR FILL
GRAPHIC LINES
PARTICLE TRACKING
HARD COPY
RETURN
0.162E+03
0.158E+03
0.154E+03
0.150E+03
0.146E+03
0.141E+03
0.137E+03
0.133E+03
0.129E+03
0.125E+03
0.121E+03
0.117E+03
0.112E+03
0.108E+03
0.104E+03
0.999E+02
0.958E+02
0.916E+02
0.875E+02
0.833E+02
0.792E+02
0.750E+02
0.709E+02
0.667E+02
0.626E+02
0.584E+02
0.543E+02
0.501E+02
0.460E+02
0.418E+02
0.377E+02
0.335E+02
0.294E+02
0.252E+02
0.211E+02
0.169E+02
0.128E+02
0.861E+01
0.446E+01
0.311E+00
MACH NUMBER
MIN= 0.15E+00 MAX= 0.16E+03
File name:
n45end

$\alpha = 10°$

Step	Circulation	Velocity at Trailing Edge	vte_n-vte_o	Circulation Total
1.	-8.045033	1.693659	1.693659	-8.04503
2.	-0.045166	0.095086	1.598600	-8.49670
3.	2.324405	-0.489339	0.584425	-6.17229
4.	0.512229	-0.107836	0.381504	-5.66007
5.	-0.522321	0.109960	0.217296	-6.18239
6.	-0.167020	0.035162	0.074798	-6.34941
7.	0.164452	-0.034621	0.069783	-6.18495
8.	0.110841	-0.023335	0.011286	-6.07411
9.	0.014399	-0.003031	0.020304	-6.05971
10.	0.020284	-0.004270	0.001239	-6.03943

Theoretical value from lifting-line theory, $\Gamma = -5.527$

$\alpha = 45°$

Step	Circulation	Velocity at Trailing Edge	vte_n-vte_o	Circulation Total
1.	-32.80016	6.905169	6.905169	-32.80016
2.	- 1.69336	0.356490	6.548679	-34.49352
3.	9.61061	-2.023249	2.379739	-24.88291
4.	2.10102	-0.442448	1.580802	-22.78125
5.	- 2.18368	0.459802	0.914639	-24.96162
6.	- 0.74310	0.156440	0.302577	-25.70472
7.	0.59641	-0.125558	0.281998	-25.10831
8.	0.35513	-0.074763	0.050795	-24.75318
9.	- 0.06019	0.012680	0.087444	-24.81337
10.	- 0.05458	0.014895	0.022156	-24.86795

Theoretical value from lifting-line theory, $\Gamma = -24.87$

Appendix 4.

Convergence Data For Both
Test Cases.

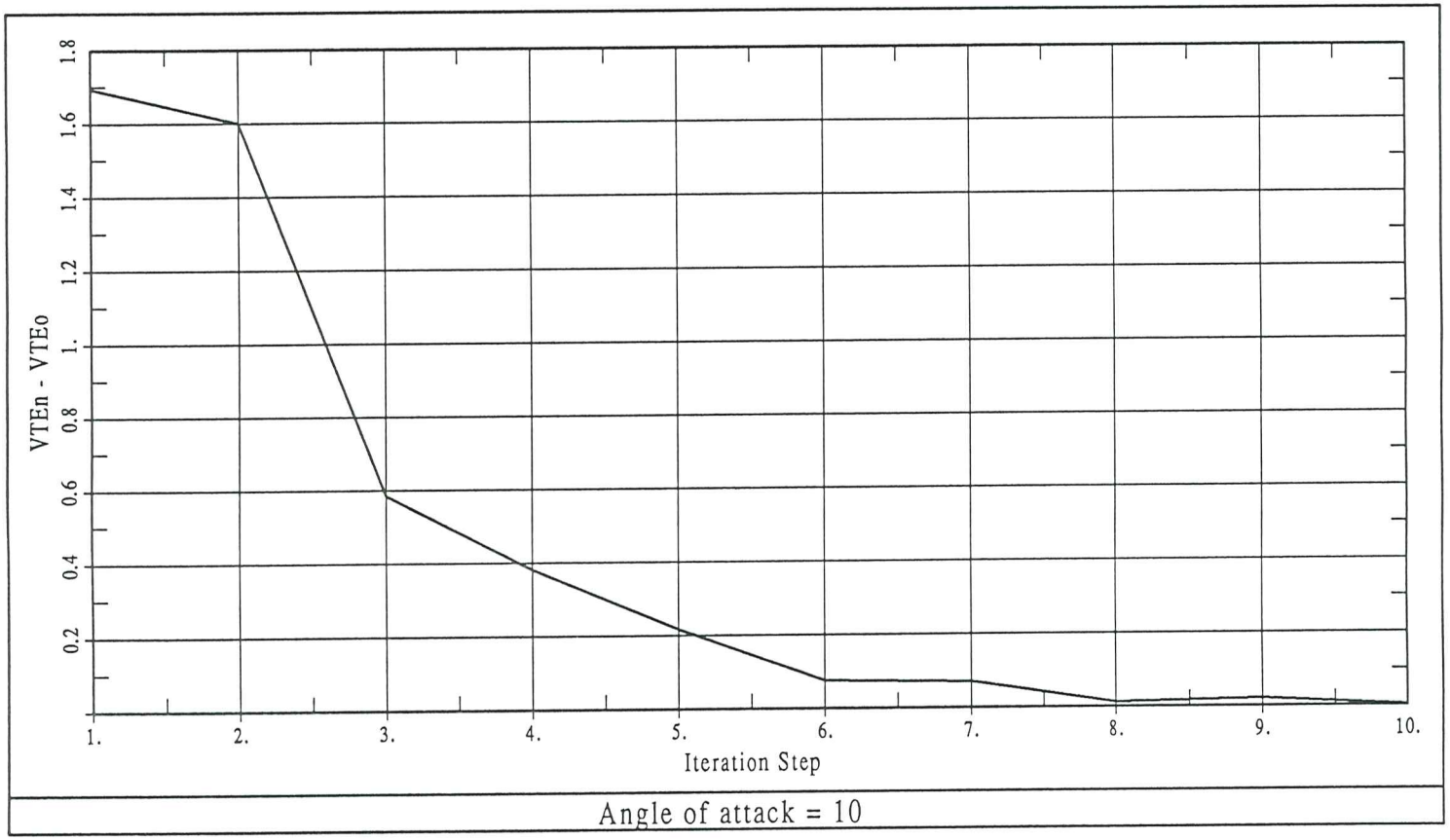

Angle of attack = 10

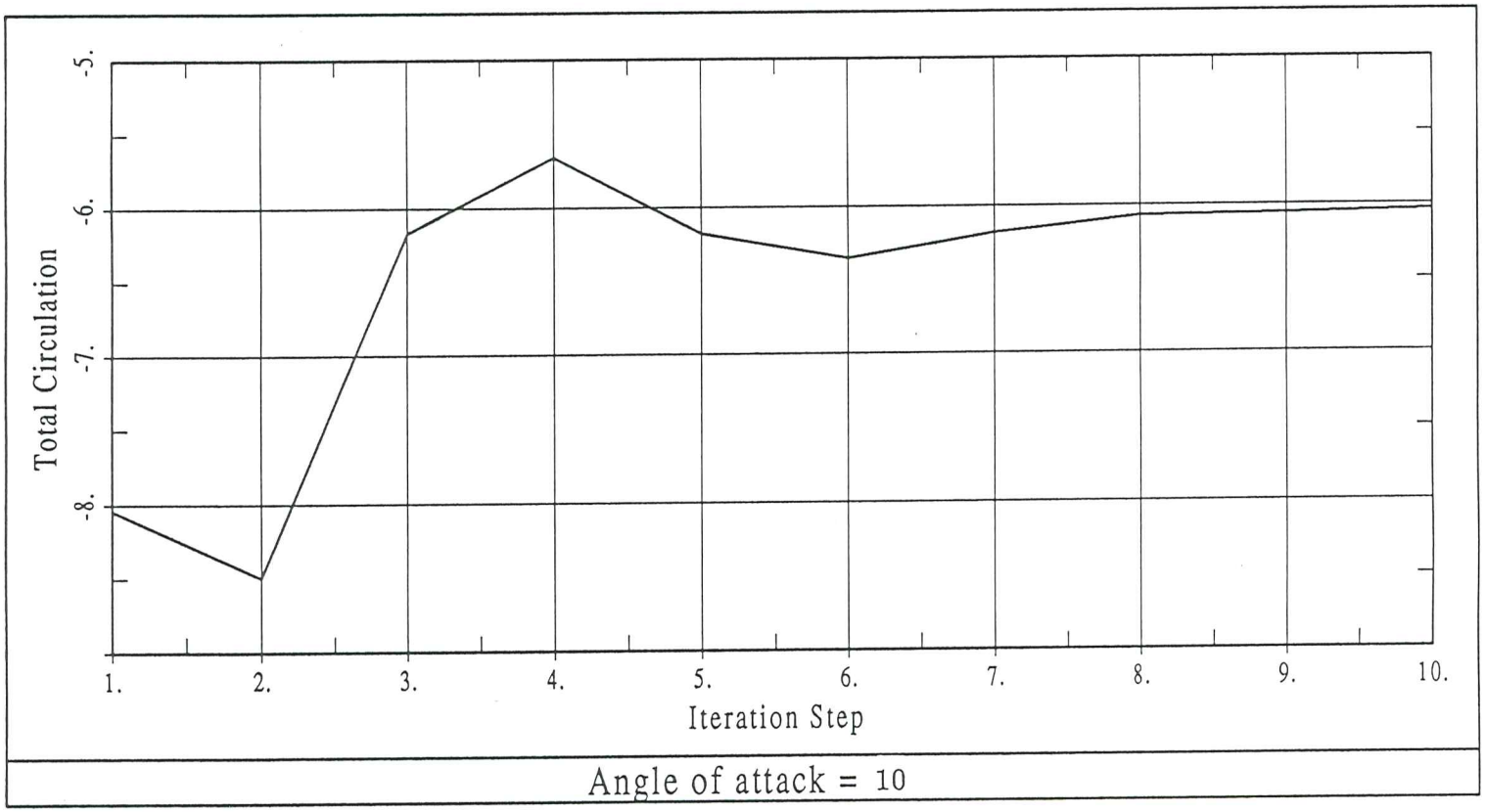

Angle of attack = 10

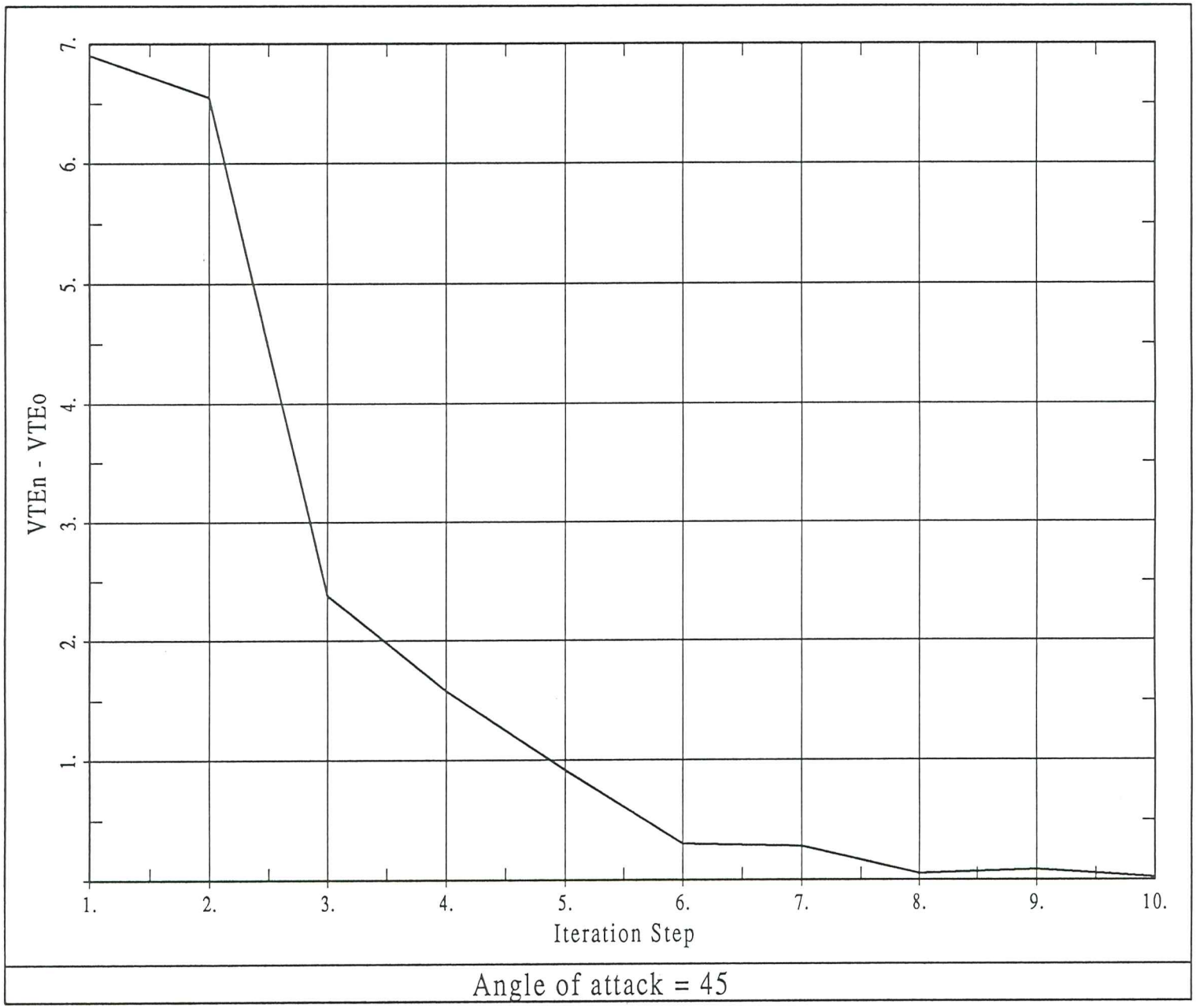

Angle of attack = 45

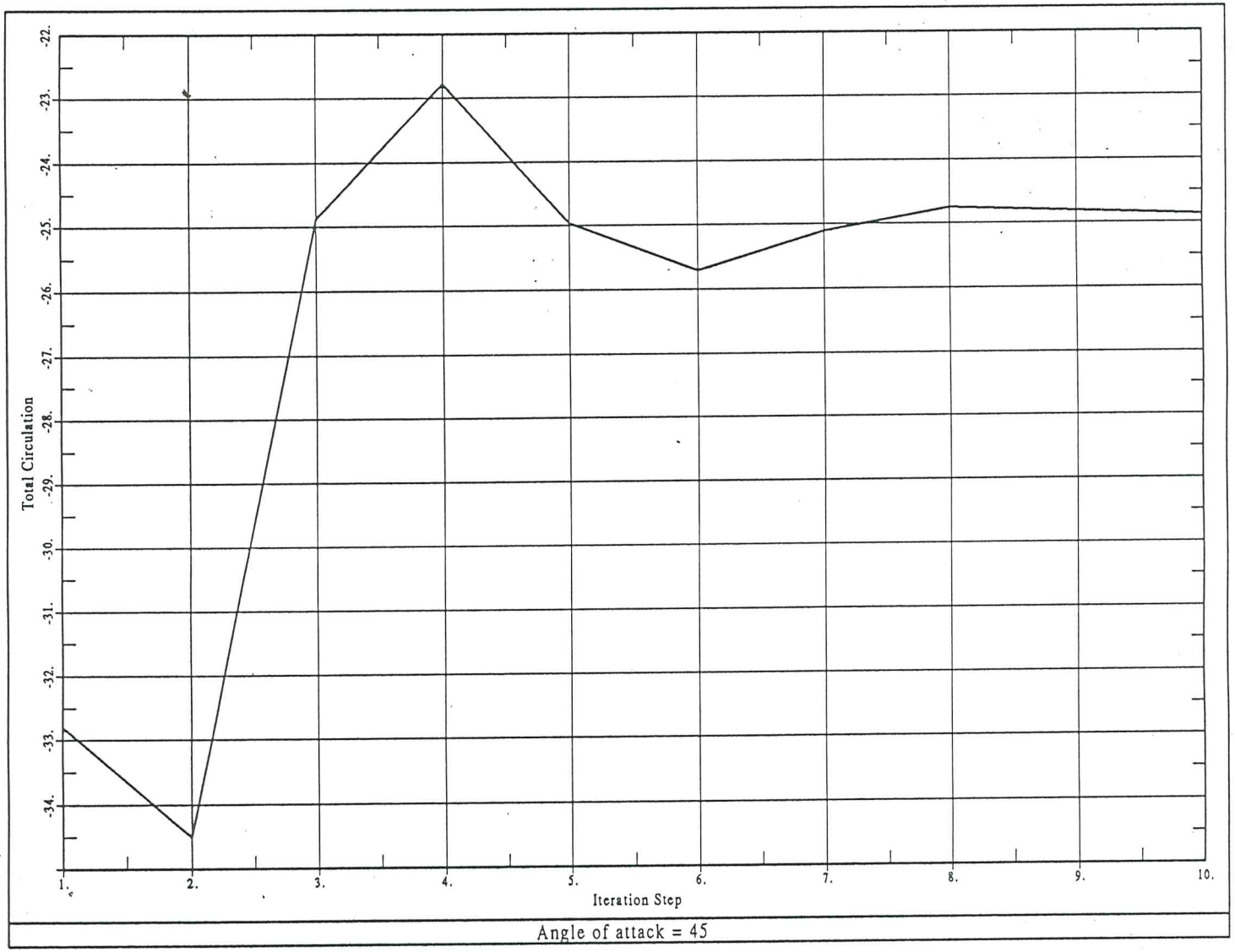

Angle of attack = 45